The Effect of Pellet Geometry on The Specific Activity of Ni-63

A Thesis Presented for the
Master's of Science Degree
The University of Tennessee, Knoxville

Spenser Riley Walsh
May 2013

DEDICATION

This thesis is dedicated to the two people who have always been the two constants in my life, my Mom and Dad. To my Dad, who has told me every day of my life I was destined for great things and whose belief in me has far surpassed even my belief in myself. He is also the one who pushed me into nuclear engineering. To my Mom, who has always reminded me that through Christ, ALL things truly are possible. Finally, to my sister who through it all - always had my back.

"For myself, faith begins with a realization that a supreme intelligence brought the universe into being and created man. It is not difficult for me to have this faith, for it is incontrovertible that where there is a plan there is intelligence--an orderly, unfolding universe testifies to the truth of the most majestic statement ever uttered--'In the beginning God." – Arthur Compton, Nobel Prize-winning physicist for his discovery and explanation of the change in the wavelength of X rays when they collide with electrons. Compton effect confirmed the dual nature of electromagnetic radiation as both a wave and a particle.

ACKNOWLEDGEMENTS

Dr. Lawrence Heilbronn has been the ideal thesis supervisor and mentor whose sage advice, wisdom, and encouragement aided in the writing of this thesis in innumerable ways. I would also like to thank Saed Mirzadeh whose steadfast support of this project was greatly needed and deeply appreciated. A huge thank you to Julie Ezold for tough love and encouraging me to reach my goals. I'd also like to thank her for forcing me to learn how to program. Also, thank you to Rose Boll who introduced me to my absolute love for radioisotopes, and for teaching me all her wisdom in the laboratory. I will always attribute the start of my career to her. Thank you as well to the entire faculty in the nuclear engineering department for sacrificing your time to teaching me. Thanks to ORNL and DOE for making it possible for me to be here.

Of course, thank you to my family and friends who prayed for wisdom and perseverance in my research and writing.

ABSTRACT

^{63}Ni [Nickel-63] is routinely produced at HFIR with a specific activity of ~15 Ci/g [Curies/gram] by irradiating highly enriched stable ^{62}Ni [Nickel-62] (86.31 %) for 2 years. Impurities in the original material are also activated and must also be accounted for, as well as removed through anion and cation exchange columns. The main goal is to investigate if a greater specific activity can be achieved by reducing target thickness axially (i.e. neutron depletion), thus reducing neutron interaction within the target interior. Because of rather high neutron capture cross-section of ^{62}Ni (σ_{th} [cross-section] = 14.5 barns, and I^0 [resonance integral] =6.6 barns), it is thought that in removing the center of the target, more ^{63}Ni activity can be produced per mass of material. To experimentally test this, three sets of solid ^{62}Ni targets were prepared of varying thickness; a solid pellet with O.D. [outer diameter] of ~6 mm and two targets in form of rings with 6 mm O.D. and 2 and 4 mm I.D. The results obtained from those targets will be presented, along with model calculations of neutron depletion in the targets with a 3D Monte Carlo simulation, part of the SCALE package.

TABLE OF CONTENTS

LIST OF TABLES

LIST OF FIGURES

CHAPTER I
INTRODUCTION AND GENERAL INFORMATION

^{63}Ni Background

1.1.1 Uses

^{63}Ni is a pure beta-emitting isotope with a 100 year half-life, and a max beta particle energy of 65.9 keV. ^{63}Ni's important characteristics are summarized in Table 1. Such characteristics, combined with its lengthy half-life, make ^{63}Ni a very promising radionuclide that can be used for several purposes. For instance, it aids in the detection of explosives, serves as a isotope source in voltage regulators and current surge protectors in electronic devices, and is also used in electron capture detectors for gas chromatographs [1]. It is particularly important for electron capture detectors where halogenated organics, nitro and amine groups are exceptionally suitable for this method of detection. In the case of electron capture detection, ^{63}Ni comes in the form of a foil, activity ranging from 10-15 mCi [2].

^{63}Ni's most promising role is in the national security arena because it can be used to in high sensitivity detection to detect explosives, chemical weapons, and narcotics. Specifically, when incorporated into security devices, it emits a beta particle, which makes it capable of acting as an ionization source, thereby enabling electrons to be stripped from molecules given off by a particular material. The resulting ions are then analyzed by the device, which can identify whether a hazardous material is present [1].

The isotope also exhibits potential for use in miniature self-sufficient power sources, providing the capability to provide a service life of thirty (30) years. Although there are a few other candidates that offer the same beta voltaic power, none provide the same service life as ^{63}Ni. As an example, tritium and promethium, which only provide about five to ten (5-10) years service life. ^{63}Ni is also superior in this regard because of its 66 keV max beta energy; it will not surpass the threshold of radiation damage for semiconductor converters. [3]. In addition, ^{63}Ni is unique in that it does not have any accompanying gamma-ray radiation or strong bremsstrahlung and an average beta spectrum of roughly 17 keV. Based upon the foregoing, neither bremsstrahlung nor beta radiation would penetrate through the battery case [3]. Because of the biological damage that beta radiation has on the human body, this ensures the safety of the safety of the general population.

Table 1. Nuclear Data used for the analysis of ^{63}Ni

Production Scheme	$^{62}Ni(n,\gamma)^{63}Ni$
Decay and Q-value	β^- 66 keV (100%)
^{62}Ni Neutron capture cross section	14.5 barns
^{62}Ni Resonance Integral	6.6 barns

1.1.2 Current Production

The utilization of ^{63}Ni is limited as a result of the small amounts being produced, which can be attributed to the extremely high cost of the product. [4] Currently, Oak Ridge National Laboratory (ORNL) is the exclusive producer of the isotope, not only in North America, but likely throughout the World.

The expensive process by which ^{63}Ni is produced is a result of neutron capture by enriched ^{62}Ni. In order to produce ^{63}Ni, one must prepare targets of highly enriched stable ^{62}Ni and bombard them with neutrons in a reactor such as the High Flux Isotope Reactor (HFIR), which has a maximum thermal neutron flux of 2.6×10^{15} neutrons/cm^2-sec, home to the world's highest steady-state neutron thermal flux. Currently, each target prepared for irradiation in HFIR contains roughly twenty-five (25) grams of pressed enriched ^{62}Ni. Once the pressed nickel is loaded into an aluminum capsule, it is bombarded with neutrons, activating the current isotope and producing a new isotope, radioactive ^{63}Ni. Because ^{62}Ni is not naturally abundant, occurring at 3.6% in nature, an enriched ^{62}Ni must be used. ORNL currently uses an enriched 96% Ni material in order to construct the targets. Because of such high enrichment, the end product is one of higher specific activity. The industry presently requires a specific activity of 15 Ci/g of target material. In order to accomplish this, the targets must be irradiated in the reactor for 15 reactor cycles. A HFIR reactor cycle refers to the total period of operation over the lifetime of the reactor core fuel element. The fuel is then replaced at the end of each cycle. The process is lengthy, with just one cycle covering a period of approximately twenty-three (23) days, with an additional nineteen (19) days of maintenance required between each cycle for maintenance. A typical ^{62}Ni target will be in the reactor for two years. After the 15 reactor cycles, a total of 375 curies of ^{63}Ni is typically produced. Because of its long half-life, the amount of ^{63}Ni produced in the target that is lost to decay is negligible, however, the burn-up cross-section of ^{63}Ni itself is rather significant and that limits the specific activity of ^{63}Ni produced in a nuclear reactor [1].

CHAPTER II
OBJECTIVE

2.1 Project Description

In order to maximize the production of ^{63}Ni, and optimize its cost, one must articulate a solution to solve the obstacles facing ^{63}Ni production. Thus, the primary goal of this thesis is to explore target geometry and determine if a target's geometry has any effect on its specific activity. By reducing target thickness radially i.e. reducing neutron attenuation within the target interior, a greater specific activity will be produced. By removal of the interior of the target, this in turn will allow for additional Ni material to be used for the construction of more pellets. Therefore, by reducing thickness, the result is additional specific activity of ^{63}Ni produced by using less material, thereby resulting in a less expensive end product.

In this study, a comparison will be made between the specific activity of irradiated solid pellets and two sets of annular rings of different dimensions. It is hypothesized that after irradiation, a higher specific activity (activity per unit mass) of ^{63}Ni will be produced in the annular rings, rather than the solid pellets. This is attributed to the high neutron capture cross-section of ^{62}Ni (σ_{th}= 14.5 b, and I^0=6.6 b), which will result in higher specific activities in the ring targets due to the mitigation of flux depression. After this is tested experimentally, it will then be verified analytically with the use of several functional models under the SCALE package. The experimental results obtained, combined with the simulated results, will prove that annular ring targets will produce a higher specific activity than solid pellet targets. This principle, in turn, can then be applied to isotopes of other interest for future research

2.2 Project Summary

This project covered many aspects involved in the production of ^{63}Ni at HFIR, including preliminary calculations, pellet fabrication, pellet irradiation, post-irradiation processing, analytical calculations, and computer simulation of the target within the reactor to verify the experimental results.

2.2.1 Target Composition

The enriched ^{62}Ni target material used for this particular experiment is produced with electromagnetic separators (known as Calutron) located within the Y-12 site [1] and then shipped to ORNL where it is kept with the ORNL Isotope Program enriched stable isotope inventory until preparations have been made for pellet fabrication. Note that Calutron is permanently shut down. Unlike the standard enriched 96% ^{62}Ni routinely used for activation, this experiment will use a target material that is 86.2% enriched. An enriched material of 96% was not used in this experiment due to costs. However, the use of 86.2% enriched nickel material will still provide adequate enrichment in order to ensure a higher specific activity, as well as fewer impurities within the target. The isotopic composition of the 86.2% ^{62}Ni, batch 204226, used for this experiment, in shown in Table 2.

Table 2. Isotope composition of enriched Ni target material

Isotope	Atom%
58	8.31 ± 0.16
60	4.60 ± 0.07
61	0.48 ± 0.01
62	86.31 ± 0.25
64	0.30 ± 0.01

Because ^{62}Ni material contains small amounts of impurities, preliminary calculations and post-processing analysis must be adjusted to account for impurities within the material. The official ^{62}Ni, batch 204226 assay, shown in Figure 2. From the assay, preliminary calculations were made to determine starting amounts of all materials, including all Ni isotopes, as well as major impurities. All of these calculations are important to consider in the activation in materials when irradiated in the HFIR. From this batch, six (6) individual target pellets were constructed, each of different size, which will be detailed further in the following section.

Figure 1. 1000 mg of Ni material for pellet construction

ASSAY

Element: Nickel
Symbol: Ni
Isotope: 62
Series:
Batch: 204226

ISOTOPIC ANALYSIS

Isotope	Atomic Percent	Precision plus/minus
58	8.31	0.16000
60	4.60	0.07000
61	0.48	0.01000
62	86.31	0.25000
64	0.30	0.01000

The limits quoted above are an expression of the precision of this measurement only. The error is estimated at less than 1% from known sources of systematic errors.

Internal Use Only
Date Entered: 02/19/2003
Last Change: 11/26/2003 06:35:12 AM
By: MFG

SPECTROGRAPHIC ANALYSIS (SSMS)

Element: ppm	Element: ppm	Element: ppm	Element: ppm
Ag: <9.0	I: <.2	Rh: <.4	Tc:
Al: 17.0	In: <.5	Ru: <.4	Te: <.5
As: <.1	Ir: <.4	S: 68.0	Th: <.3
Au: <.8	K: 56.0	Sb: <.3	Ti: 28.0
B: 6.0	Li:	Sc: 2.0	Tl: <.4
Ba: 26.0	Mg: 10.0	Se: <.2	U: <.3
Be: .6	Mn: 25.0	Si: I	V: 82.0
Bi: <.3	Mo: <.5	Sn: <1.0	W: <.8
Br: <.2	N:	Sr: 5.0	Zn: 11.0
C:	Na: 1.0	Ta: <2.0	Zr: 2.0
Ca: 190.0	Nb: <.1		
Cb: <.1	Ni: M		
Cd: <.5	O:		
Cl: 42.0	Os: <.6		
Co: <.2	P: I		
Cr: 740.0	Pa:		
Cs: <.2	Pb: 18.0		
Cu: 47.0	Pd: <.5		
F: <.3	Pm:		
Fe: 27.0	Po:		
Ga: <.5	Pt: 39.0		
Ge: <4.0	Ra:		
Hf: <.9	Rb: <.4		
Hg: <.9	Re: <.4		

LANTHANIDES and ACTINIDES

Am:	La: 76.0
Bk:	Lu: .8
Ce: 71.0	Md:
Cf:	Nd: 82.0
Cm:	Np:
Dy: 3.0	Pr: 19.0
Er: <7.0	Pu:
Es:	Sm: 3.0
Eu: .6	Tb: .7
Fm:	Y: 40.0
Gd: 5.0	Yb: 2.0
Ho: .7	Tm: <.2

* Symbols: M - matrix; S - support; T - trace; I - interference;< - less than; </= less than/equal to; nd - not detected.

* Request No. A-0738; Log # 4875; Notebook No. A-107329-L, pgs. 280 - 283.
* <- No spectrum line visible. Probably absent, definitely less than value given.
* <T- Present but less than value given.
* The spectrographic results reported herein are semi-quantitative estimates and should not be interpreted or construed to be precise quantitative determinations.

Figure 2. Target material assay obtained from the ORNL Isotope inventory

2.2.2 Target Geometry

Of batch 204226, six (6) individual ^{62}Ni specimens were formed, each of their own specific dimension. Because batch 204226 is a powder material, the process consisted of pellet fabrication, including forming, sintering, and pressing them into their corresponding shape. In order to test the hypothesis of this thesis, there were three different size shapes constructed; 2

solid pellets, two 2-mm inner diameter ring specimens, and two 4-mm diameter ring specimens. Pellet geometry can be seen in Figures 3-8

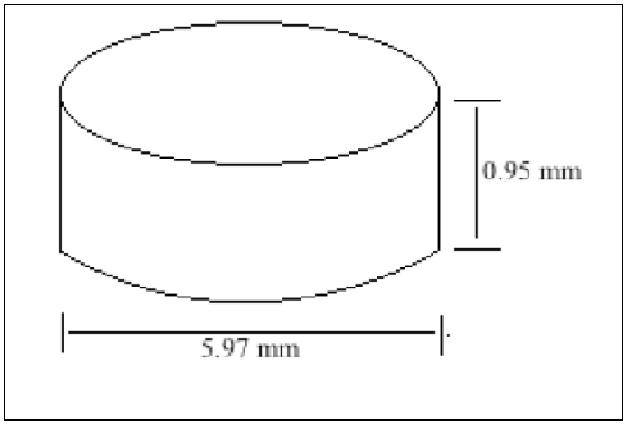

Figure 3. Solid #1 dimensions

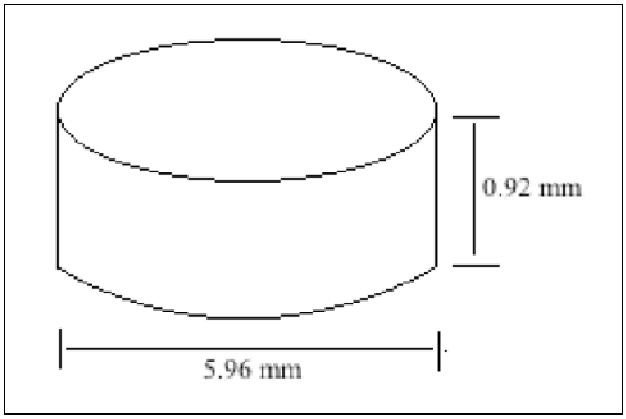

Figure 4. Solid #2 dimensions

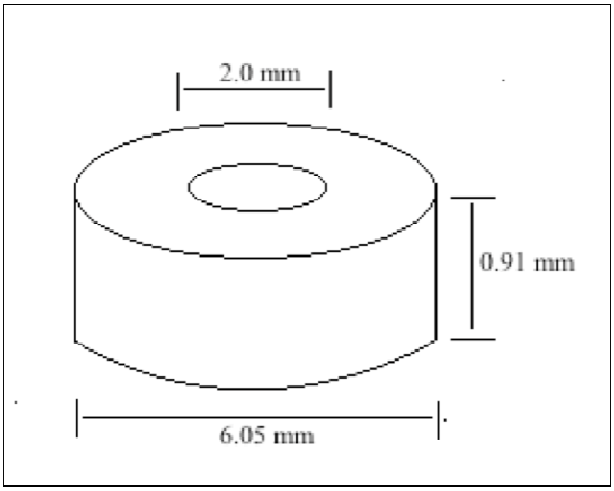

Figure **5. 2-mm I.D. #1 dimensions**

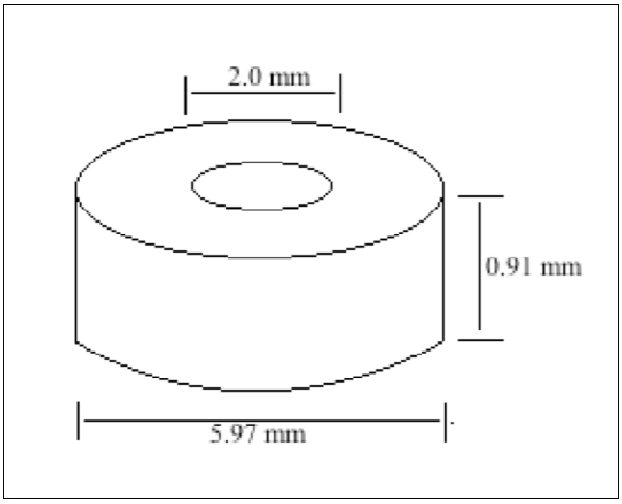

Figure 6. 2-mm I.D. #2 dimensions

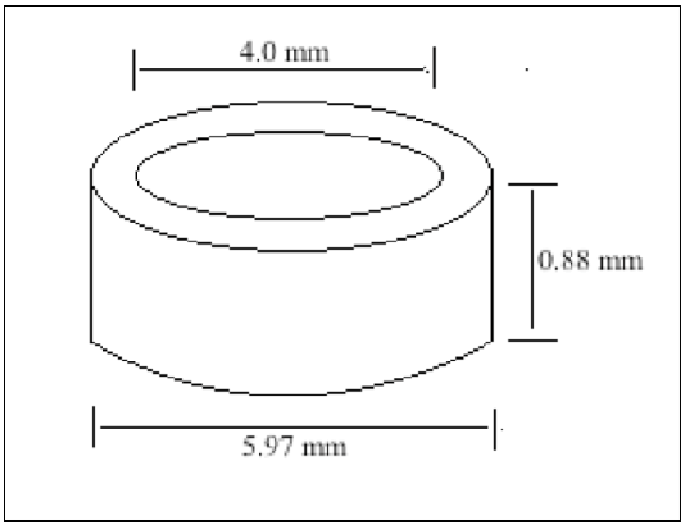

Figure 7. 4-mm I.D. #1 dimensions

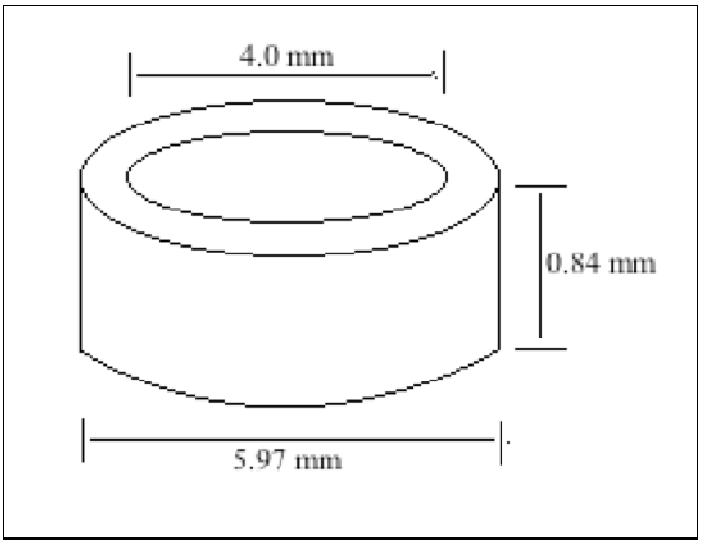

Figure 8. 4-mm I.D. #2 dimensions

CHAPTER III
MATERIALS AND METHODOLOGY

3.1 Pellet Fabrication and Irradiation

3.1.1 Pellet Fabrication from ^{62}Ni powder

Fabrication of the pellet and rings consisted of first grinding 1000-mg of the ^{62}Ni (enriched 86.31 %) into a powder from batch 204226 stored in the Isotope building at Oak Ridge National Laboratory. For future reference, a procedure was constructed so that pellet fabrication could be duplicated. Each pellet was constructed by following the procedure:

1. Clean dish and mortar with 1:1 8 M Nitric Acid (HNO_3), and allow soaking for 5 minutes.
2. Remove dish and mortar from HNO_3 and rinse with ethanol (CH_3CH_20H) twice to ensure a clean surface, free from impurities.
3. Remove the 1000 mg of ^{62}Ni powder in several increments and grind to a fine powder-like substance using the clean mortar and dish.
4. Clean a quartz boat with HNO_3 to ensure an impurity-free surface and set aside.
5. Pour the ground bits of ^{62}Ni powder into the quartz boat.
6. Use a brush to remove nickel remnants from dish into quartz boat.
7. Wash dish and mortar with ethanol to see any visible ^{62}Ni remnants.
8. Place quartz boat, containing ^{62}Ni powder, into Thermolyne 79300 high-temperature quartz tube. (This will remove the amount of oxide present so that the nickel will press more efficiently into pellets or rings). The Thermolyne quartz tube can be seen in Figure 11.
    a. First, run Argon gas through the tube in order to clear the air out for 5 minutes
    b. Reduce the Argon gas to a minimum, then place tube into furnace chamber
    c. Flow pure Hydrogen through tube for ~5 minutes to flush the argon and change the atmosphere to Hydrogen.
9. Turn furnace on using the control switch to 750°C, heat the tube for 45 minutes and switch to Ar and allow the furnace to cool overnight.
10. After an overnight cooling, remove Nickel from the Thermolyne tube furnace. (A gray color indicates the lack of oxide).
11. Weigh the Ni powder (which turned out to be 0.9874 grams). Retrieve the residue from evaporated dish (equaled 0.0005 grams in this run). Add the residue to the powder (total combined amount here was 0.9879 grams).
12. Using a Dake 50 ton hydraulic hand-operated press, use 6000 lbs. of pressure to press each die in which the nickel resides.

Figure 9. ^{62}Ni powder in quartz bowl and tantalum boat prior to Thermolyne furnace placement

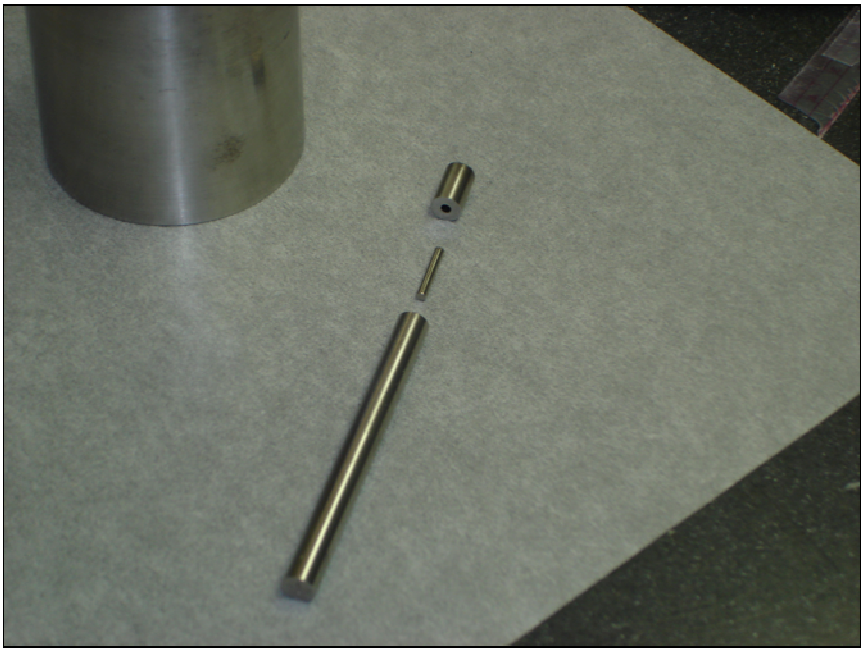

Figure 10. Die used in combination with Dake press for specimen

At the completion of this procedure, a total of six pellets were constructed; two solid pellets, two 2-mm. inner diameter ring specimens, and two 4-mm inner diameter ring specimens.

After pellet fabrication, each was weighed and measured. Their individual properties can be seen in Table 3.

Table 3. Pellet dimension after pellet fabrication from ^{62}Ni powder

Pellet Size	Weight	Final Weight (g)	Thickness	Diameter (mm.)
Solid #1	0.1951	0.1948	0.95	6.03
Solid #2	0.1956	0.1954	0.95	6.03
2 mm ID #1	0.1783	0.1778	0.94	6.03
2 mm ID #2	0.1788	0.1785	0.94	6.03
4 mm ID #1	0.1018	0.1077	0.86	6.03
4 mm ID #2	0.1091	0.1088	0.90	6.03

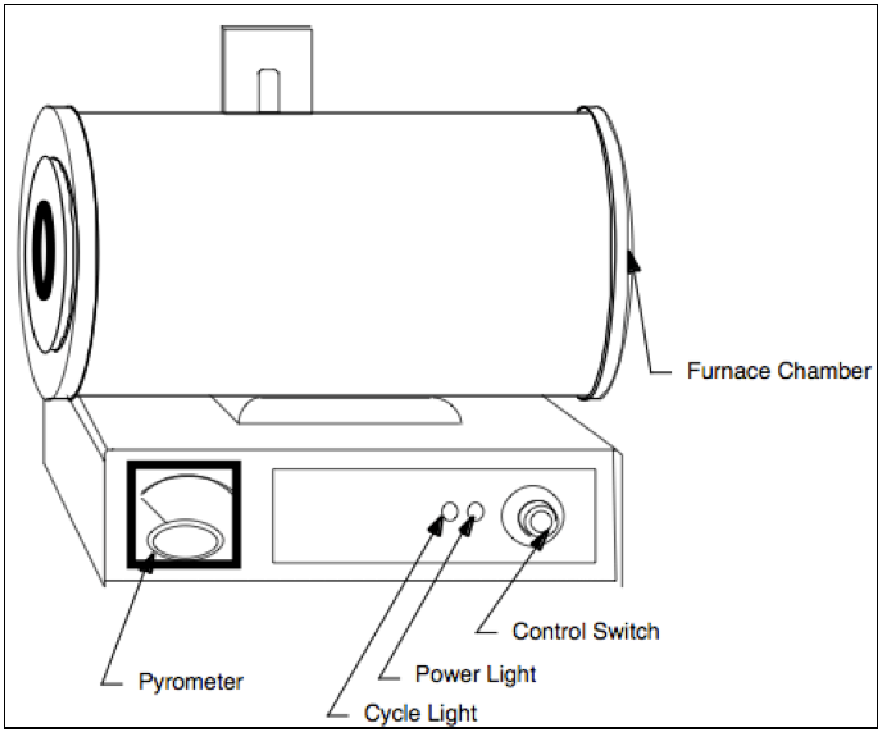

Figure 11. Furnace chamber diagram [8]

Figure 12. Thermolyne 9300 Furnace

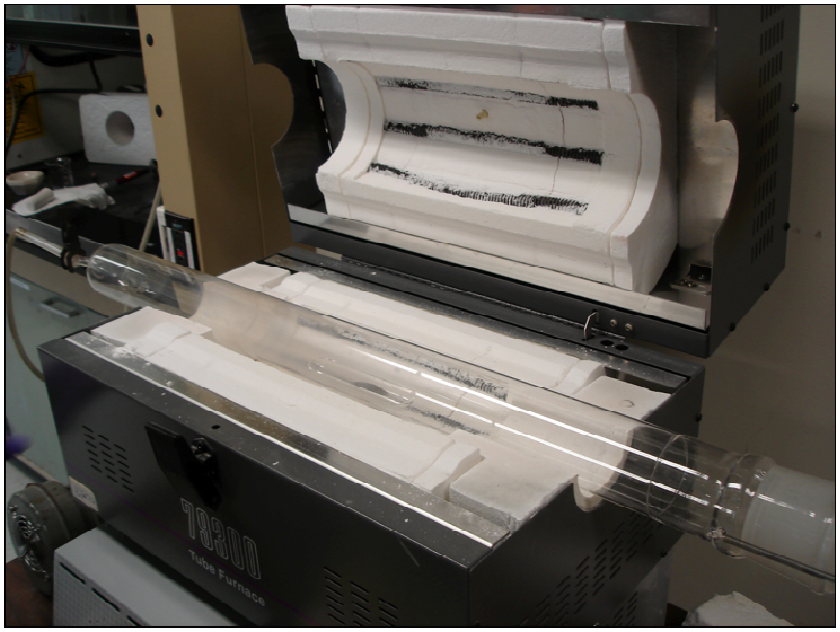

Figure 13. Interior of Thermolyne Furnace where pellets were oxidized

3.1.2 Pellet Sintering

The pellets were then placed into a Tantalum boat, which was then placed into a sintering furnace. The purpose of sintering the pellets was to fuse the particles of the specimens together, to ensure the mechanical stability of each individual pellet. Sintering was conducted in vacuum at a total pressure of ~10^{-4} Torr (mm of Hg). The sintering procedure was as follows:

1. Sinter the pellets in the sintering oven.
2. Turn on the Vacuum pump and when pressure drops to ~10^{-4} Torr, heat to 150 °C for 15 minutes.
3. Hold at 1000 °C, which will take ~2 hours.
4. Hold at 1000 °C for 3 additional hours, then allow to cool.
5. Retrieve pellets and weigh each.

After the pellets were sintered, it was necessary to re-weigh each in order to get a more precise measurement. The final dimensions of each pellet can be seen in

Table 4. Final pellet dimensions post-sintering, prior to irradiation

Pellet Size	Weight (g)	Thickness (mm.)	Diameter (mm.)
Solid #1	0.1936	0.92	5.96
Solid #2	0.1943	0.95	5.97
2 mm. ID #1	0.1774	0.91	6.05
2 mm. ID #2	0.1767	0.91	5.97
4 mm. ID #1	0.1079	0.88	5.97
4 mm. ID #2	0.1069	0.84	5.97

Figure 14. Sintering Furnace fuses the Ni particles of each pellet

3.1.3 Preliminary Analytical Calculations

In order to determine what was expected from the irradiation of a set amount of ^{62}Ni, it was essential to develop and perform calculations. Additionally, impurities in the original material were activated, thereby must be taken into account. The initial anticipated amounts of material were processed both by analytical calculations, as well as utilizing 2-D modeling software developed at ORNL called IsoChain. Utilizing the two methods of calculation, the expected activities were calculated. However, calculation only predicted the activity based on 2-D assumptions. Therefore the specific activity of each was, as expected, the same. Using the basic decay equation 1 and the fixed variables based on the flux of HFIR and ^{62}Ni absorption cross-section, one can model the expected activity (and mass) of produced ^{63}Ni after a 2-hour

irradiation. Additionally, the same equation was applied in order to also calculate the amount of impurities that would be activated as well.

$$\frac{dN'}{dt} = \phi\sigma N_T * (1 - e^{-\lambda t}) \quad (1)$$

Where,

$\frac{dN'}{dt}$ = Activity of N'_T, ^{63}Ni (disinegrations/sec)

ϕ = Flux (neutrons/cm^2-sec)

σ = Cross Section (cm^2 or b) 1 b = 10^{-24} cm

N_T = Atoms in target of ^{62}Ni

λ = Decay constant of ^{63}Ni (sec^{-1})

Table 5. Expected specific activity and mass of 63Ni in each pellet

Pellet Size	Expected Specific Activity of ^{63}Ni (mCi/g)	Expected Mass of of ^{63}Ni (g)
Solid #1	10.23	3.54 x 10^{-5}
Solid #2	10.28	3.58 x 10^{-5}
2 mm. ID #1	10.29	3.25 x 10^{-5}
2 mm ID #2	10.29	3.24 x 10^{-5}
4 mm ID #1	10.29	1.98 x 10^{-5}
4 mm. ID #2	10.29	1.96 x 10^{-5}

In theory, the specific activities of each pellet predicted by analytical calculations should be of equal values because this calculation does not account for the flux depression or take into consideration the geometry of each individual pellet or ring. The corrections for flux depression and consideration for the target geometry will be addressed in the Neutron Shadowing section (3.3) of this thesis. The purpose of these calculations was theoretically to provide the amounts of activity that could be expected before taking into account neutron attenuation, as well as to provide HFIR management with adequate proof to ensure that the target would not adversely affect the operation of the reactor.

3.1.4 Aluminum Rabbit Configuration

The six individual specimens were placed in a hydraulic aluminum encased 'rabbit' marked NM-802, designed specifically for irradiation of small samples in the hydraulic tube irradiation facility of HFIR. The standard finned aluminum rabbit has an inner diameter of 6.55±. 076 mm and is 60 mm in length.

Figure 15. Aluminum "rabbit" marked NM-802

3.1.5 Target Loading

The six ^{62}Ni specimens were placed in alternating order, with quartz glass spacers in-between each. The ends were stuffed with a small ball of quartz glass wool. A depiction of the target can be seen in Figure 16, with specified dimensions and placement.

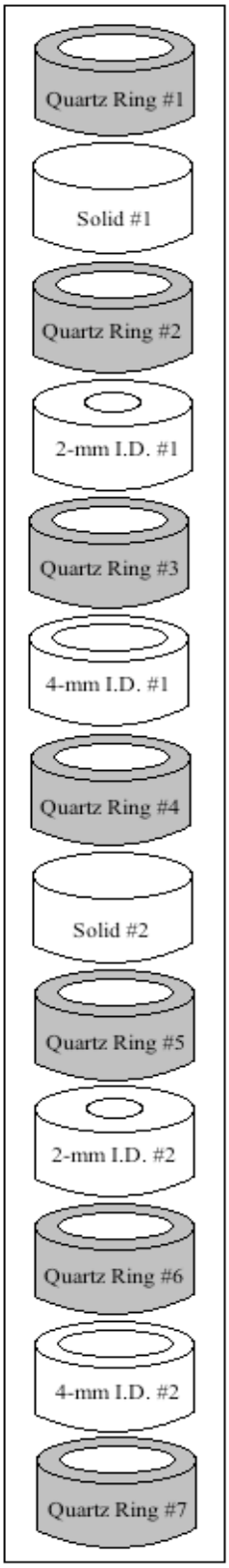

Figure 16. Interior of aluminum rabbit showing the positioning of the target

3.1.6 Preliminary Pre-Load Tests

After the aluminum target was welded shut and before the encapsulated targets were placed into the HFIR, safety precautions were taken as the target had to undergo a multitude of tests to ensure that it was sealed and safe for irradiation. These included the following tests, of which will each specifically be discussed. Each of these tests was performed with the help of David Denton and Saed Mirzadeh, who are approved by HFIR to sign the corresponding test documentation.

- Helium Leak Test: Was performed in order to confirm the reliability of the welded aluminum target by checking for the presence of leakage in the capsule. The target was first helium bombed for one hour with the use of a cylindrical vacuum chamber, where it was first placed and pumped down to -20 PSI. The vacuum valve was then closed tightly, proceeding with the opening of the helium valve from He supply tank. The chamber was pressurized to 90 psi with He and allowed to stand for one hour. Then, He was removed from the chamber. After being bombed with helium at 90 psi for one hour, the capsule was then placed into the chamber of a Leybold PheonixL 300 (He leak detection system). The detection system contained mass spectrometer, which enables the measure of He ions. Following QA instructions, the target was tested recording the helium leak rate which was below allowable limit of a He leak rate of $1x10^{-7}$ STD He atom per sec. he target passed this test.
- Hydrostatic Pressure Test: This test was performed in order to replicate the circumstances the target would be subject to when placed in the HFIR. The target was placed into the pressure chamber, which was filled with water and sealed. The chamber was pressurized to 1100 psi, and then released to 600 psi ten times. After completion, the chamber was depressurized, and the target was taken out.
- Oven Test: After removal from the pressure chamber, the target was placed into the laboratory oven, where it was kept overnight at 120 ^{o}C for one hour. Each capsule would be weighed and if the weight had increased or decreased by more than 10 milligrams, would be rejected as to indicate water had entered into the capsule.
- Bubble Test: The final test to ensure the absence of large leakage was to perform the bubble test, which would submerge the capsule in water and apply slight negative pressure (from house vacuum) to observe the presence or absence of bubbles. No bubbles were observed, thus the target passed the test.

3.1.7 Preliminary Target Temperature, Heat Load, and Thermal Expansion

Additional calculations had to be made as part of HFIR QA requirements in preparation for target irradiation and to perform heat calculations to ensure that once the targets were loaded into the aluminum capsule thermal expansion of the pellets would not occur, placing stress on the aluminum rabbit when irradiated in the High Flux Isotope Reactor. The target temperature, heat load and thermal expansion of nickel are bounded by two previous analysis for tungsten targets; C-HFIR-2007-002 entitled “Tungsten Rabbit Irradiation in the HFIR Target Region”, and C-HFIR -2002-035, entitled “Tungsten Cylinder Target Temperatures in

the HFIR Hydraulic Tube", and Ho-166m target C-HFIR-2008-028 entitled "Holmium Cylinder Target Temperatures in the HFIR Hydraulic Tube". The decay heat in the Ni target is by far smaller than that in the W target. The primary product of the neutron irradiation of ^{62}Ni is long-lived ^{63}Ni ($t_{1/2}$ =100 y), produced by ^{62}Ni [n,□]^{63}Ni reaction with thermal and resonance cross-sections of 14.5 and 6.6 barns, respectively. In comparison, the primary product of the neutron irradiation of ^{186}W is 1-d ^{187}W, produced by ^{186}W [n,□]^{187}W reaction with a thermal and resonance cross-sections of 37.9 b and 484 b. The Q_{β}- and average beta energy of ^{63}Ni are 66 and 17.1 keV, and that for ^{187}W are 1312.5 and 274 keV, respectively. The gamma heating of Ni is somewhat smaller than that of W, ~54 W/g whereas W is 64 W/g. The melting point of Ni is 1453^{o}C, about half of that for tungsten, 3387^{o}C. At room temperature, density and thermal conductivity of Ni is also about a half of that for tungsten, but the Specific Heat and the Coefficient of Linear Thermal Expansion of Ni is about three times larger than that for tungsten. A comparison of some physical properties of W and Ni is given in Table 6.

Table 6. Comparison of W and Ni metal to ensure negligent thermal expansion

Physical properties	Target (metal)	
	W	Ni
Melting point (^{o}C)	3422	1453
Density (g/cm3)	19.3	8.908
Thermal conductivity @100^{o}C (cal/(s.cm. ^{o}C))	0.40	0.198
Specific Heat @ 200 ^{o}C (Cal/g)	0.032	0.1225
Coefficient of linear thermal expansion, (K^{-1})	$4.5x10^{-6}$ @ 25^{o}C $5.8x10^{-6}$ @ 1000^{o}C $5.92x10^{-6}$ @ 1400^{o}C	$13.4x10^{-6}$ @ 25^{o}C $20.6x10^{-6}$ @ 1000^{o}C $24x10^{-6}$ @ 1400^{o}C
Q_{β}- (MeV)	1.3125	0.06587
Gamma Heating (@ 100 MW)	64 W/g	~54 W/g
Av. Beta Energy (keV)	274	17.1
Av. Gamma-ray Energy (keV)	430	-

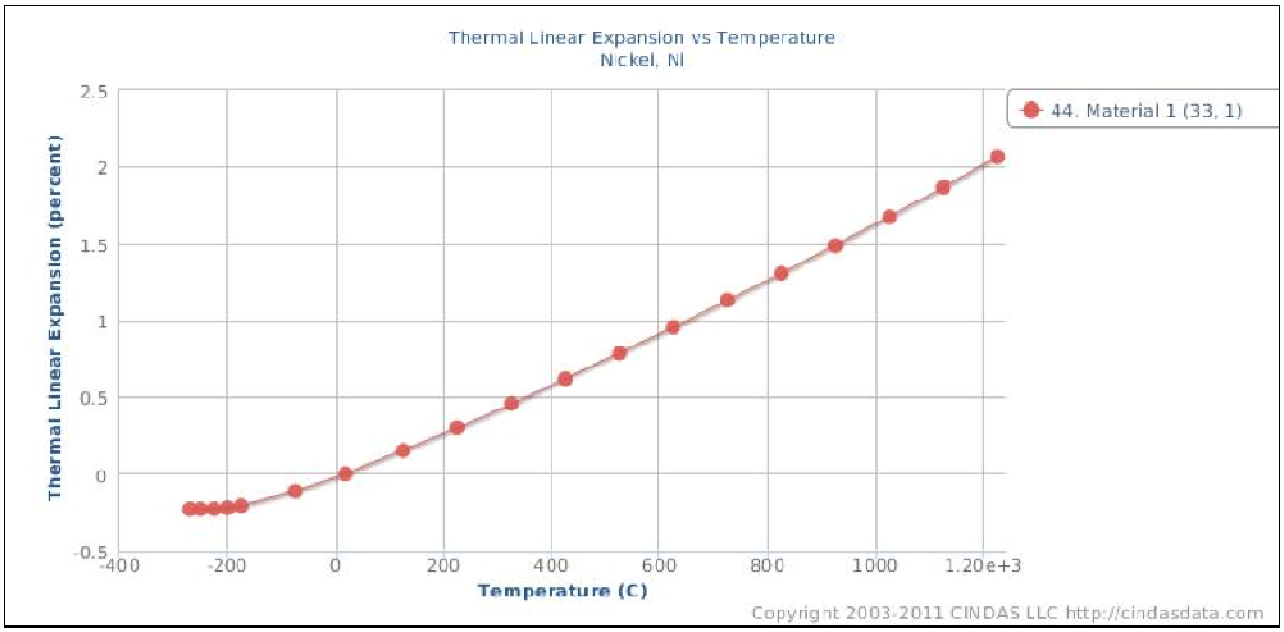

Figure 17. Thermal Linear Expansion vs. Temperature of Ni

From the data presented in the proceeding section, it is evident that with regard to the decay heat, target mass and amount of radioactivity produced, the approved tungsten and holmium targets (Heat calculations: C-HFIR-2007-002, C-HFIR -2002-035 and C-HFIR-2008-028), bounded the nickel target (NM-802). The only remaining issue was the larger expansion coefficient of Ni relative to that of W, which may result in a possible stress on the Al rabbit housing. There will not be any stress on the Al housing even at a temperature just below the melting point of Ni (1435^{o}C). The standard finned Al rabbit has an inner diameter of 6.55±. 08 mm. From data presented, it is evident that at a temperature just below melting point, the Ni thermal linear expansion is less than 2.5%. Applying a thermal linear expansion of 2.5% to the 6.05 mm O.D. ring (this is the ring with the largest diameter, and conservatively assumed that the ring is a solid pellet) results in an absolute linear expansion of 0.15 mm, therefore the pellet diameter would increase to a maximum of 6.20 mm at 1453^{o}C (just below melting point), leaving a 0.35 mm linear gap (or 0.17 mm radial gap) between the pellet O.D. and the Al housing I.D. The gaps would be slightly larger for other three rings and two solid pellets which all have slightly smaller outside diameters than 6.05 mm. Therefore one can conservatively argue that nickel pellets and rings within the NM- 802 aluminum rabbit do not apply any stress on the Al housing at any operating temperature. This verified the safety of the irradiation of the target in the HFIR.

3.1.8 Target Irradiation

After the required QA and necessary documentation was completed, the target was irradiated at 10:52 AM on 7-9-2011 at position #5 in the Hydraulic Tube region for 2 hours during

Cycle 436, while reactor was operating at 80 MW. After discharge, the target was allowed to cool in the reactor pool.

3.1.9 Target Removal

After cooling, the irradiated target was transported from HFIR to a glove box in Room 127 in building 4501 in a lead pig on 8-3-2011. A lead pig was crucial in order to have sufficient shielding during transportation. The target was taken out of the lead pig within the lead shield, where it read about 150 mRem just outside of the lead glass shielding. The Al capsule was then cut open at the end cap with a pipe cutter, and the cap was placed back into the lead pig for further shielding. Six separate glass containers were labeled to accommodate each individual pellet. The quartz wool was removed with a pair of tweezers with a bent angle tip, which ensured easier removal. The three quartz glass rings were removed, each of the pellets were removed, and then placed into their corresponding glass containers and capped. Each container was pushed to the back of the glove box to minimize dose, and read about 1.5 mRem just outside of the lead glass shielding.

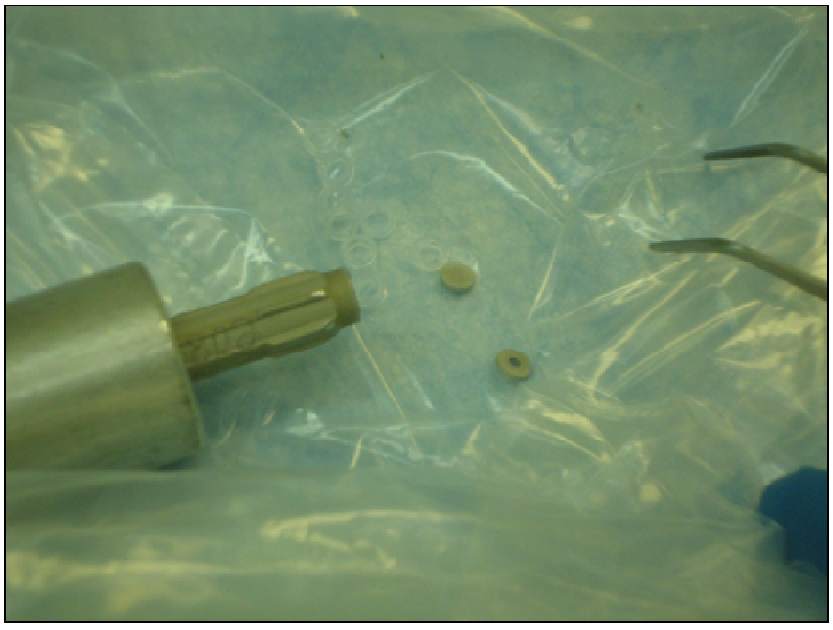

Figure 18. Irradiated NM-802 in the glove box preparing for pellet dissolution

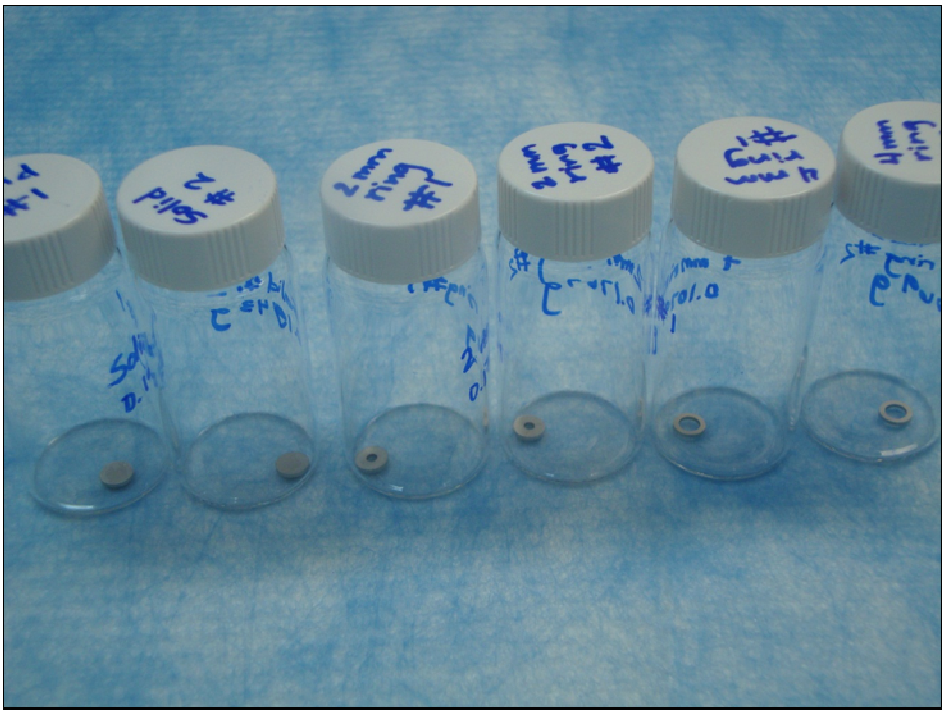

Figure 19. Unpacked pellets from NM-802 preparing for pellet dissolution

3.1.10 Post-Processing Dissolution

Prior to any separations, it was first necessary to convert each solid specimen into a liquid state for post-processing purposes. A unique procedure was followed for pellet dissolution:

1. Pipette 2 mL of 3 M NaOH into each glass container containing the pellets and allow to soak for 1.5 hours. This ensures the removal of any Aluminum residue left on each specimen.
2. Add 1 mL 8 M HNO_3 and set on hot plate.
3. Add 1 mL of 8 M HNO_3 to each pellet and allow to sit for fifteen minutes.
4. Add 1 mL of 8 M HNO_3 and observe to ensure no reaction taking place. (If bubbling or color change observed, turn the hot plate down)
5. Add 2 mL H_20 to bring the known volume up to 5 mL

The same process was carried out for each target specimen. Dissolution was important to the post-processing because it was necessary to convert each pellet to a liquid state in order to perform the anion column separations, which would be carried out to remove impurities.

Figure 20. Solid #1 in dissolution

Figure 21. Solid #1 as time elapsed during specimen dissolution (notice color change)

3.1.11 Post-Processing Anion Exchange Column

Anion and cation exchange columns were built and used in order for post-irradiation processing. The anion exchange column is intended for the removal of all transition metals, excluding nickel and chromium. The cation exchange column process follows the anion

exchange process and serves to strip chromium from the solution. However, after observing this process, it was seen that this did not adequately remove the Chromium from the solution therefore, the anion exchange column was the only post-processing tool utilized following dissolution. The procedure for each dissolved pellet was as follows:

1.) Take 0.5 mL of dissolved nickel and take to dryness with the help of a hot plate.
2.) Add 1 mL of 9 M HCl while container is on hot plate and take to dryness again to dissolve previous nitric acid from prior dissolution.
3.) Redissolve in 0.5 mL 9 M HCl
4.) Build a column using 100-200 column resin of MP1 (Chloride). Make the column resin 0.5 mL
5.) Load 0.5 mL of dissolved nickel solution.
6.) Wash column 3 times with 0.5 mL of 9 M HCl.
7.) Collect wash and load into one vial and label "L1" for a total of 2 mL
8.) Wash column with 3-4 bed volumes of 4 M HCl and collect into a vial labeled "W1" 9.) Strip column with 3 bed volumes of H_20 and collect in a vial labeled "E1".

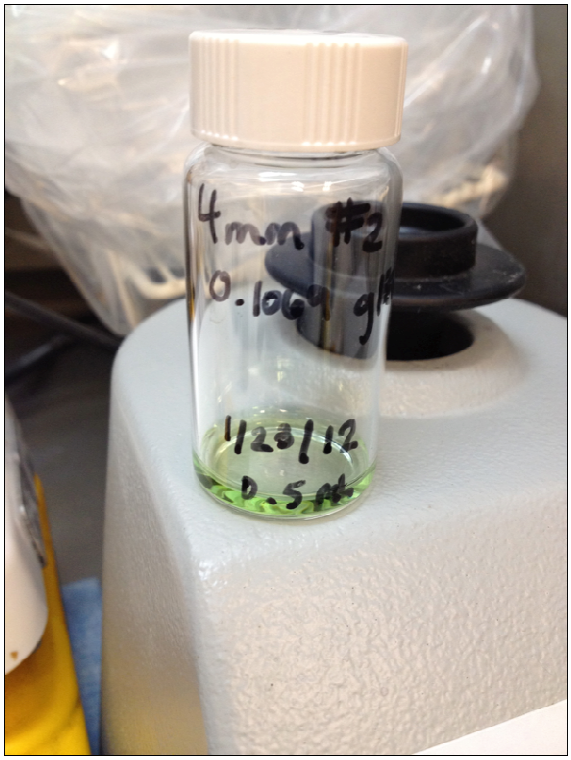

Figure 22. Dissolved 4-mm I.D. #2 ring specimen

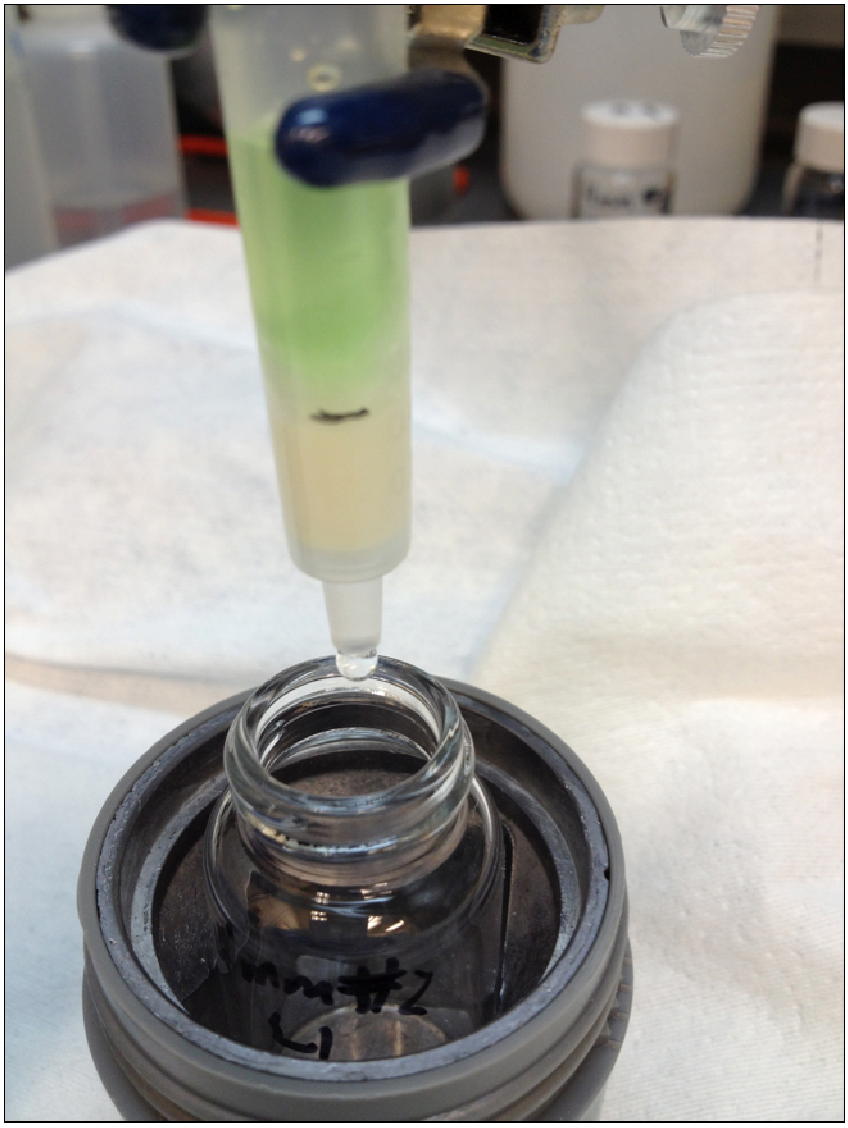

Figure 23. Anion exchange column

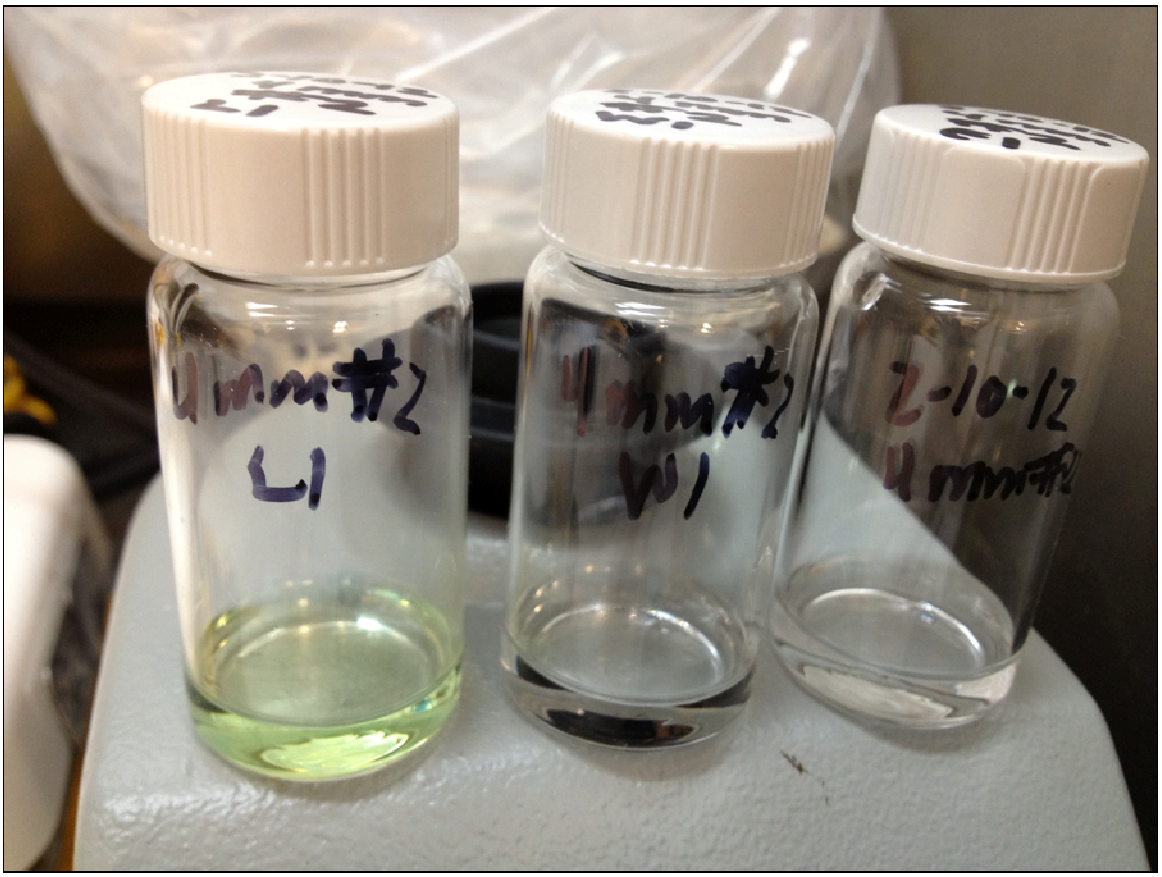

Figure 24. Sample solutions during anion column process

3.1.12 Chemical and Analytical Science Division (CASD) Processing

Because ^{63}Ni is a beta emitter, samples were analyzed utilizing mass spectrometry in order to determine the ^{63}Ni content. A sample of 0.5 mL of the load solution was sent for analysis. Because a beta particle has a continuous energy spectrum, identification of pure beta particle emitters can be problematic .Beta particle emitters have a sharp energy spectrum, thus the most commonly used techniques to count beta emitters are gas filled counters such as a Geiger Muller or liquid scintillation.

The method of detection for this work was liquid scintillation, which was performed by the Chemical and Analytical Science Division. Liquid scintillation counting is a process which takes advantage of the way in which particles transfer energy to matter *without* causing ionization. Liquid scintillation trusts wholly on this principle to measure how much of a radionuclide is existent [17]. The dissolved radionuclide is first mixed with a “cocktail”, which is a mixture of a particular solvent and scintillator (fluor). The decay energy of the beta is then transferred to the cocktail, converted to photons, and then counted using a photomultiplier tube. By counting the photons, the activity of the radionuclides can then be determined [18].

CASD reported an activity/mL with ±10% error from each sample solution, where a dilution factor was then applied to each. A total activity was then calculated and knowing the mass of each pellet provided a specific activity. These results will be discussed in the Results section of this paper.

3.2 HFIR Theory

In order to better understand the phenomena occurring with specimen irradiation and activation, it is necessary to understand the HFIR theory.

3.2.1 HFIR Basics

HFIR is a light-water cooled, beryllium reflected, 85-MW producing flux-trap type reactor [19]. HFIR is responsible for producing the world's highest, steady state thermal flux in the world, 2.6×10^{15} neutrons/cm^2-sec. The core of the reactor consists of several concentric annular regions (each of which is 61 cm. high), one of which includes the "flux trap", which is home to 37 vertical experimental target sites. [3]. A picture of the reactor core of HFIR can be seen in Figure 25. The flux trap is of particular importance because it houses the placement of the target irradiated. [3]. Encasing the flux trap are two concentric fuel elements, separated by a water region. The inner fuel is highly enriched uranium oxide, while the inner region consists of ^{10}B, which serves as a burnable poison. The average life cycle of the core is anywhere from 22 to 24 days, operating at 85 MW [3].

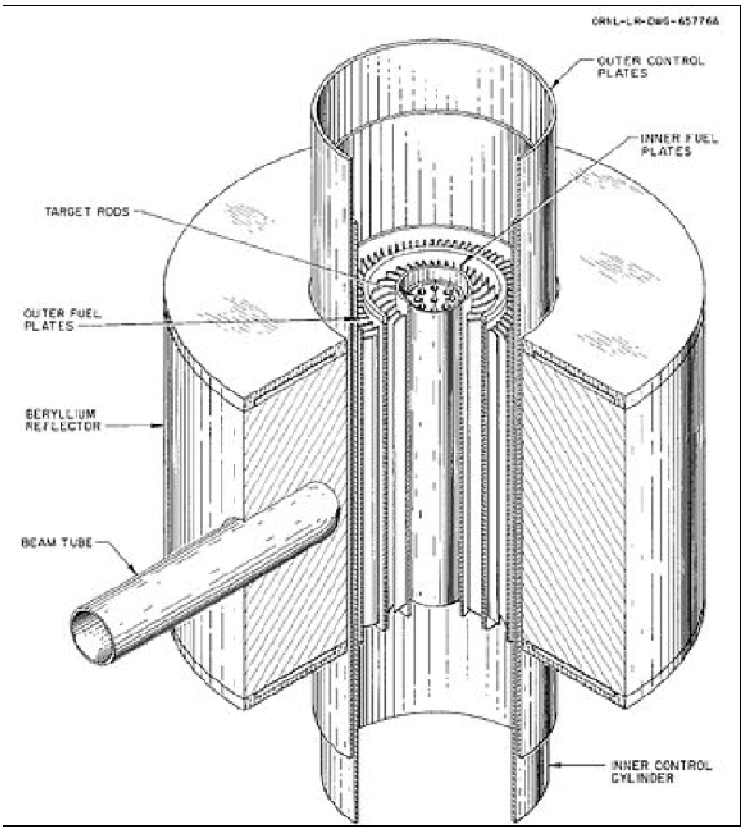

Figure 25. HFIR reactor core

3.2.2 HFIR Flux Trap

Within the reactor core is an area designated the flux trap. There are a total of thirty-one positions in the flux trap. While at one time these positions were originally intended for target rods used to produce transplutonium elements, they have also become useful in other experiments. [3] These positions are of importance because they provide the highest thermal neutron flux. The location of the flux trap within the reactor core can be seen in the cross-sectional view of the core in Figure 4.2.

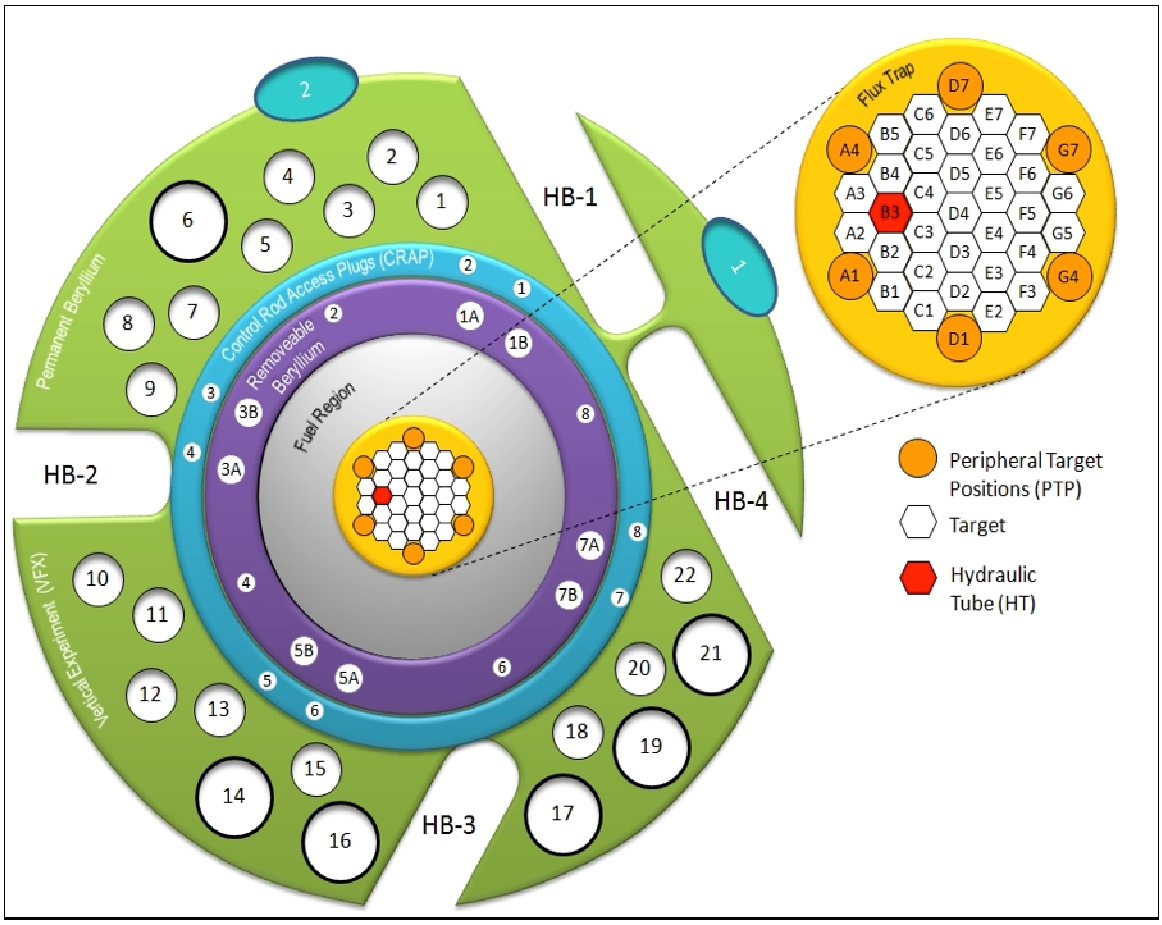

Figure 26. Sketch of the flux trap within HFIR

3.2.3 HFIR Hydraulic Tube Facility

Reference Figure 26, highlighted in red is the hydraulic tube region. The hydraulic tube region is of the area of most concern in the irradiation of the ^{62}Ni target. The uniqueness of this region is its capability to irradiate certain materials for a period of time that is less than the reactor's cycle [4]. This enables a train of small capsules, rabbits, to be inserted in and out of the core on demand. This made it ideal for the irradiation of the constructed ^{62}Ni target, whose irradiation time was two hours. The flux trap region can be illustrated in Figure 4.3, with HT marked where the hydraulic tube is located.

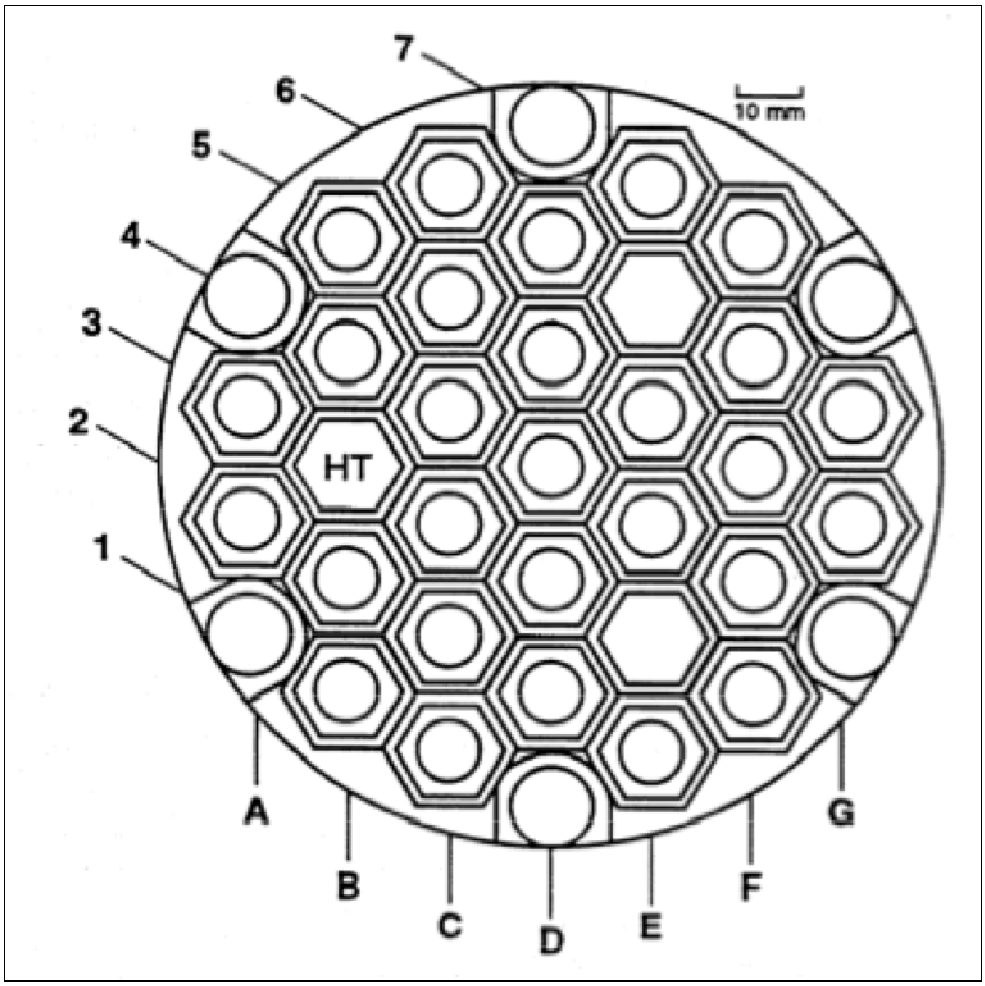

Figure 27. Flux trap region of HFIR

3.3 Neutron Shadowing

3.3.1 Neutron Interactions

Because the simulation is dependent on occurrences in the HFIR, it is necessary to understand the behavior of neutrons and activation within the reactor. A neutron carries no charge therefore it will interact via direct nuclear interactions with the atomic nucleus, thus excluding electromagnetic interactions with the electron cloud. The main types of neutron-induced reactions are scattering reactions and absorptions. These are further broken down into subcategories, which can be observed in Figure 28. When a neutron collides with a nucleus, the scattering can be elastic in that the total kinetic energy is conserved or it can be inelastic in that the nucleus will absorb some internal energy and is then left in an excited state. Fast neutrons will generally lose energy by means of elastic events. As the neutron begins to lose energy, the scattering will continue, but the probability that capture occurs increases [6].

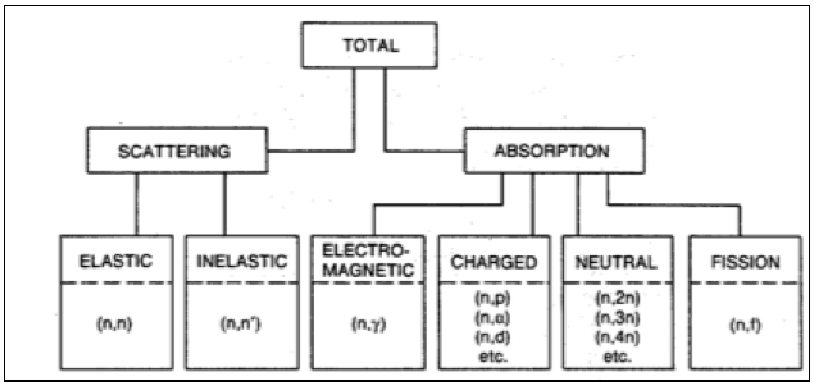

Figure 28. Subcategories of neutron interactions by scattering and absorption mechanisms

How a neutron behaves in a particular interaction is dependent upon the neutron cross section. The neutron cross section symbolizes the probability of a particular event occurring between a neutron and the nucleus of an atom. It is possible when a group of neutrons are incident on a material, they may interact, (thereby changing their direction and energy), have no interaction and continue through the material, or fail to emerge from the material. Each of these events can be described by the concept of a neutron cross section. These probabilities will determine the manner and probability in which the neutron will behave with a particular nucleus [10].

Referring back to the basics of neutron interaction, how a neutron interacts can be applied to neutron cross sections. It is known that a neutron will interact with an atom either through a scattering event or an absorption event. This prospect is expressed through the microscopic cross section. The likelihood of a neutron being absorbed by a particular atom is referred to as the microscopic absorption cross-section, denoted σ_a. Complementary to this is the microscopic scattering cross-section, denoted σ_s, which is simply the probability that a neutron scatters off a nucleus. Corresponding to Figure 28, each of these can likewise be broken down further. The scattering events include both inelastic and elastic events, thus, can be represented by the following equation:

$$\sigma_s = \sigma_e + \sigma_i \qquad (2)$$

where

σ_e = elastic events

σ_i = inelastic events

The microscopic absorption cross-section includes all events with the exception of scattering events. It is adequate to separate neutron interactions into two sub-categories, neutron capture and fission. Therefore, the following equation is used to sufficiently represent the probability of all absorption events. However, the fission aspect will not be utilized for this thesis.

$$\sigma_a = \sigma_c + \sigma_f \qquad (3)$$

where

σ_c = neutron capture

σ_f= fission

In reference to the absorption microscopic cross-section, this value is generally small for many elements, however ^{62}Ni has a microscopic cross section of 14.5 barns, thus the probability of absorption is greater, thus activating the outer edges of the specimen, and depressing the flux in the center of the solid targets. This phenomena will be discussed in more detail in Section 3.3.2

These cross sections are dependent on neutron energy and also with the incident nucleus. Typically, as the energy increases, the absorption cross section will decrease. Below 1 MeV, the elastic cross section stays relatively constant, while the inelastic and absorption cross sections can be described as the reciprocal of the neutron's velocity. The cross sections at larger energies look as to have larger peaks overlaid on the 1/v trend. These are described as resonance regions and they appear at energies where the reactions are enhanced. A resonance might occur if the combination of an incident neutron and target form a compound nucleus. This phenomenon will thus display neutron energy close to the energy of the new state of the compound nucleus. Figure 29 is a good illustration of absorption cross-section vs. neutron energy for further insight into the concept of how energy plays a vital roll in the probability of interactions.

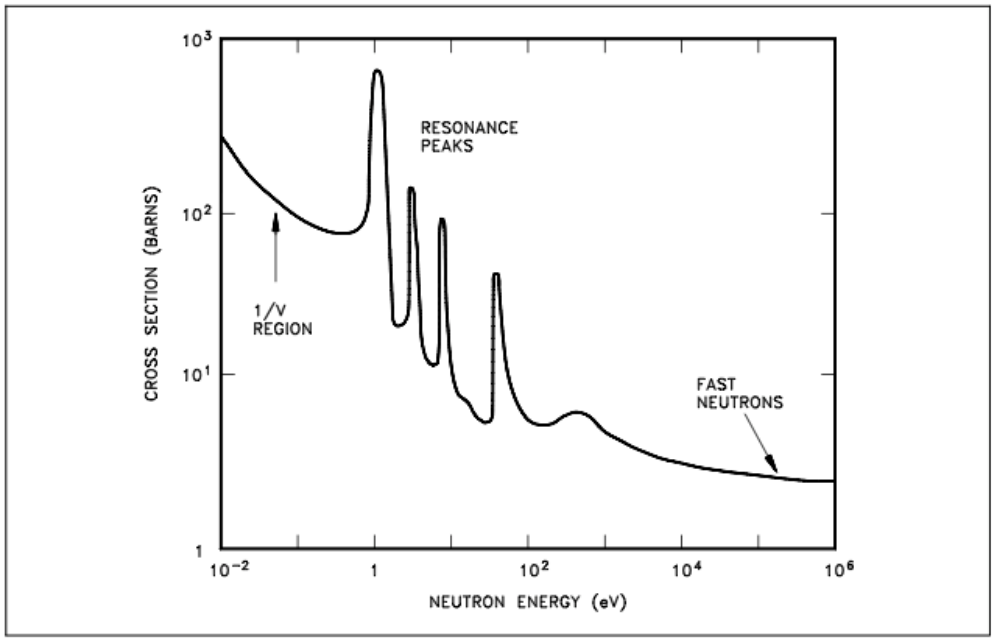

Figure 29. Absorption cross sections as a function of energy [5]

Understanding the behavior of neutrons in the HFIR, combined with the understanding of cross-sections, is crucial to understanding activation of the target, NM-802.

3.3.2 Flux Depression

The understanding of neutron interactions within HFIR can now be applied to the target, NM-802, which was irradiated in the HFIR for two hours. The hypothesis is that annular ring specimens would produce a higher specific activity than the solid pellet specimens. Because of the large absorption cross section of ^{62}Ni, increases the likelihood for neutron capture to occur, thus turning ^{62}Ni into ^{63}Ni.

$$^{62}_{28}Ni + n \rightarrow {}^{63}_{28}Ni$$

Of concern for most research and for this study are the thermal neutron absorption cross-section, and the resonance integral. The resonance integral will take into account the absorption peaks at specific neutron energies, exclusive to a particular isotope, above the thermal range, but encountered as neutron moderation takes place; That is, as a neutron begins to slow down. Because of the large thermal absorption cross-section (14.5 barns) as well as the resonance integral (6.6 barns), neutron absorption is likely. This means that upon irradiation, a thermal neutron interacts with a target nucleus (^{62}Ni) through a non-elastic collision, initiating neutron capture, thus producing the isotope ^{63}Ni, as illustrated in Figure 30.

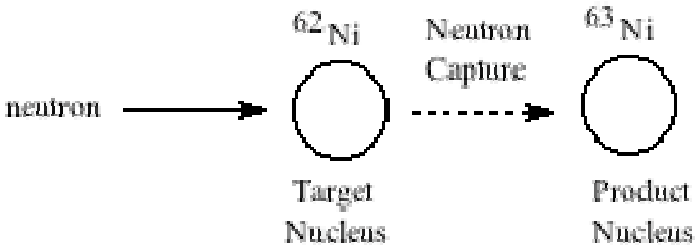

Figure 30. Illustration of production via neutron capture

A high specific activity can be achieved by irradiation of ^{62}Ni rings rather than ^{62}Ni solid pellets through removal of the center of the pellet. The advantage of this is that by removing the middle of the pellet, not only can more specific activity be achieved per unit mass, but more material is left that can be used to construct more pellets. This would not only maximize production, but minimize cost as well. This is attributed to the fact that more neutrons will interact and absorb in the exterior of the material, reducing activation in the center of the pellet. This phenomenon can be best described as “neutron shadowing” or “self shielding”. This is where the flux is significantly lower in some areas due to loss of flux in preceding areas. In other words, local neutron flux becomes depressed within a material due to the absorption of neutrons near the surface of the material. The interior of the material will experience a lower average flux than the outer surfaces due to the fact that a substantial fraction of the neutrons will be absorbed and thus never “touch” the interior. This sensation is specifically imperative at resonance energies, because of the large absorption cross-sections [5].

This occurrence can be observed in Figure 30, which shows that flux depression increases the deeper within a pellet it "travels". This is based on the equation that represents the surviving flux through the material, which is an exponential function:

$\Phi_{tr} = EXP(-N\sigma x)$

where
N = atomic density (atoms/cm^3)
σ = absorption cross-section (cm^2)
x = depth in pellet (cm)

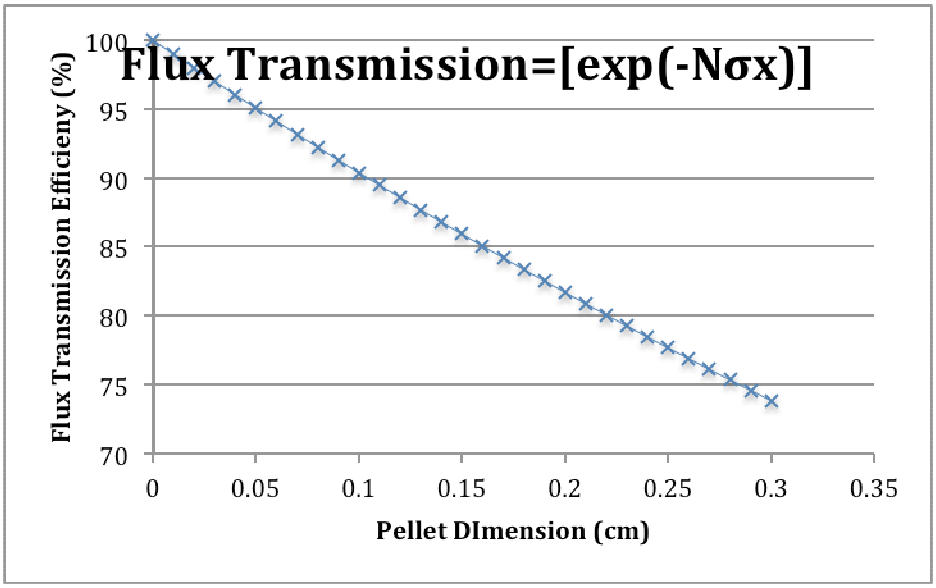

Figure 31. Thermal flux as a function of pellet depth

After the ^{62}Ni specimens are irradiated, the ring specimens should produce a higher specific activity than the solid pellet specimen if the level of neutron flux attenuation is significant. This effect was studied experimentally, as well as simulated with a depletion code, which will be further discussed in Section 3.4

3.4 Simulation Theory

3.4.1 SCALE Simulations

In order to best illustrate the self-shielding phenomena occurring within the target, it was necessary to employ a model that reflects the activation of materials through the transport and behavior of neutrons within the HFIR. In order to do this, the SCALE6.1 package (which is developed and maintained by Oak Ridge National Laboratory) was expended to perform simulations. SCALE6.1 is an inclusive collection of programs, which offers tools in order to simulate criticality safety, reactor physics, radiation shielding, and sensitivity analysis. It

consists of 89 computational modules, of these, which include 3 deterministic and 3 Monte Carlo radiation transport solvers. Included in SCALE6.1 are nuclear data libraries and processing tools for continuous and multi-group energy neutronics calculations, as well as activation and decay. Of the 89 computational modules are a few in particular of importance for the sake of this research, which perform problem-dependent cross-section processing. BONAMI, OPUS, KENO-VI, CENTRM, and WORKER are all functional modules employed in order to accurately simulate the problem. The control modules included in the SCALE package of particular interest are ORIGEN-S coupled with TRITON [19]. The next subsection will explain each module that the particular input for this thesis employed.

ORIGEN-S (Oak Ridge Isotope Generation in Scale) is a functional module within SCALE6.1 created for the sole purpose of calculating time-dependent nuclide concentrations, activities, and source terms for a multitude of isotopes simultaneously depleted by transmutations, fission, or decay. This is accomplished via solving the Bateman equations for burnup-dependent cross-sections. Simple approximations of transmutation rates can be created by solving the Bateman equations for materials that are subject to a constant neutron flux. The combination of burnup-dependent cross-sections and the Bateman equation will allow for updated isotopic number densities [9]. The rate of change of the concentration of any given nuclide can be determined (time-dependent) can be expressed analytically:

$$\frac{dN_i}{dt} = \text{Formation Rate} - \text{Destruction Rate} - \text{Decay Rate} \quad (4)$$

$$\frac{dN_i}{dt} = \sum y_{ji}\sigma_{f,j} N_j \phi + \sigma_{c,i-1} N_{i-1} \phi + \lambda'_i N_i' - \sigma_{f,i} N_i \phi - \sigma_{c,i} N_i \phi - \lambda_i N_i \quad (5)$$

where

$\sum y_{ji}\sigma_{f,j} N_j \phi$ = yield rate of N_i due to the fission of all nuclides of N_j

$\sigma_{c,i-1} N_{i-1} \phi$ = the rate of transmutation into N_i due to the radiative capture by nuclide

N_{i-1}

$\lambda'_i N_i'$ = the rate of formation of N_i due to the radioactive decay of nuclides N_i'

$\sigma_{f,i} N_i \phi$ = the destruction rate of N_i due to fission

$\sigma_{c,i} N_i \phi$ = the destruction rate of N_i due to all forms of neutron absorption other than

fission (n,γ, n,α, n,p, n,2n, n,3n)

$\lambda_i N_i$ = radioactive decay rate of N_i

This equation is written specifically for a medium that encompasses a space and energy averaged neutron flux, with corresponding average cross sections, σf and σc. The flux is a function of space, energy, and time, and will ultimately determine the nuclide concentrations, in turn determining the isotopic number densities present in each target [13].

TRITON (Transport Rigor Implemented with Time-dependent Operation for Neutronic depletion) is a control module within the SCALE package that can solve reactor design problems by providing 3D Monte Carlo depletion using KENO-VI. TRITON thus employs depletion and decay calculations with the coupling of ORIGEN-S. In order to perform these calculations, the SCALE package comes equipped with cross-section data, both continuous-energy and multigroup neutron libraries based on the ENDF/B-VII. These libraries contain decay information, cross section, and fission-product yields. TRITON utilizes KENO (t6-depl) to solve the neutron transport equation and then ORIGEN-S to deplete the materials for each depletion step defined in the burndata block of the input code [14].

KENO-VI, the main functional module that drives this code, is a three-dimensional code that uses the Monte Carlo method to solve the transport equation. Monte Carlo programs are in simple terms a calculation technique that predicts the life of a neutron with "rolls of dice", using the random numbers in a computer. This stochastic method is ideal for three-dimensional simulation because it allows the user to simulate a physical situation. It allows for the tracking of discrete particle histories and then averages them in a random walk directed by measured interaction probabilities (cross sections). Contrary to a deterministic method, which will solve the Boltzmann transport equation in a numerical approximate manner, the stochastic approach to modeling neutron transport will model the system almost exactly and solve the model statistically anywhere in the system. Many simulations are performed, which can be referred to as "histories" and the desired result is then taken as an average over that number of observations. Specifically in context to neutron transport, neutrons are "thrown" from a source at the given system, and then each is followed one by one and its various events are recorded. For example, interactions such as collision, absorption, fission, and escape are all recorded. These all combine to make up the history of one neutron [11]. Along the neutron's path, a decision is made to simulate a certain interaction, based on the cross section for the interaction with the material at particular neutron energies. In digital Monte Carlo techniques, implicit capture (which is of importance for the sake of this thesis) does not allow the particle to be absorbed, thus neutrons are assigned a weight (at one initially) and at every collision, this weight is reduced [10]. This process continues until there is no more relevance to that neutron's life, such as through moderation or escape. In turn, this is then repeated for hundreds or thousands of neutrons, depending on the input of the simulation. By repeating this, the input is able to come up with a common behavior amongst the neutrons, and can predict things of interest such as activation of materials in the HFIR [10]. There are several advantages to a stochastic approach rather than a deterministic. A deterministic will use numerical discretization methods and apply them to an ordinary or partial differential equation to describe a system. In a stochastic approach, the physical system can be modeled directly, without the need for the differential equations to be recorded in order to describe the system. The only requirement for stochastic methods is the use of probability density functions in order to describe the system. Once these

functions are known, the simulation advances through random sampling from the functions. Therefore, KENO, rather than explicitly solving the transport equation, uses the statistical nature of the transport equation to simulate particles by drawing random numbers to determine what happens to a particle from the moment it is born to the moment it dies (i.e. leave the system or is absorbed). By simulating millions of actual particles it produces the mean results (flux, k-effective) that a deterministic method would solve for explicitly. All events the neutron undergoes are tried from established PDF's, thus pinpointing the exact location, energy, and angle of the source neutron. From these details, one can explain the distance the neutron travels before a collision, from that collision whether it is absorbed or scattered, and its characteristics after a given collision. This Monte Carlo method will therefore not experience abbreviated error due to its ability to handle continuous energy, spatial, and angular variables. The disadvantage of using a Monte Carlo method is the statistical error attributed to averaging individual results from many neutrons. A deterministic method would require a solution of the Boltzmann transport equation, which can be extremely difficult regarding computations due to the fact the problem has seven dimensions: three in space, two in direction, and one in both energy and time. This method would typically require the discretization of the Boltzmann equation in every independent variable and then approximate derivative of functions using finite differencing methods. In regards to neutron transport, for example, the discrete-ordinates method, S_n, is used to discretize the angular variable. Here, the Gauss-Legendre quadrature set approximates integrals over angle. The dominant error concerning this method is spatial discretization. Contrasting, the discrete-ordinates method will contemplate an infinite number of particles in a finitely defined system, while the Monte Carlo method considers a fixed number of neutrons in an infinite system [12].

The specific input used for the purpose of this thesis utilizes all of the above functional and control modules simultaneously in order to accurately simulate the hypothesis. The flow chart seen in Figure 32 is a depiction of the process the code runs through in order to generate results.

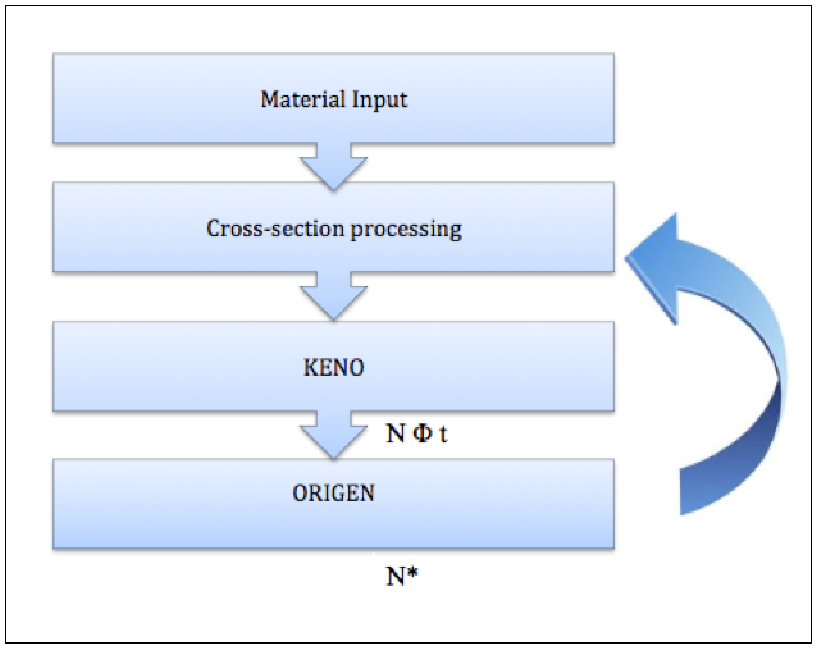

Figure 32. Flow chart of SCALE modules utilized

More specifically, the exact geometry, materials, and characteristics of the reactor core and the target, were input in order to accomplish the ultimate goal of determining the amount of activity produced by each pellet, or ring, specimen. The method of solving will be discussed in the following section.

The first step was to define the geometry and media, as to indicate where in the reactor the aluminum rabbit was placed, which housed the six individual pellets. After the materials have been read, TRITON utilizes CENTRM and BONAMI in order to perform cross section processing and self-shielding analysis. Using the cross-sections for a particular isotope, it can calculate the neutron spectrum in order to determine multi-group cross sections. CENTRM does this by solving the 1-D transport equation in order to collapse to 2-D, thus collapsing from continuous uses the transport code, tracking one particle at a time using the multi-group cross sections determined prior. From KENO, a flux and nuclide concentration are determined at t=0 (beginning of cycle). ORIGEN uses the Bateman equation, coupled with cross sections in order to determine a new nuclide concentration after a specified time interval. The cycle is thus repeated with the new nuclide concentration. After all this data, the code is able to calculate the activity of each pellet, by simple input of target material, geometry and reactor characteristics by the user.

3.4.2 Model Input

The input file for this particular thesis used an input based off of Cycle 400 of the HFIR, which started on April 27, 2004 at 2:55 a.m. and ended at precisely 5:35 p.m. on May 21, 2004. Therefore, the life of cycle 400 was 24 d, 14 h, and 40 min, or 24.61 d. The reactor operated at 85 MW during this period of time [16]. The geometry of the reactor, as well as

reactor parameters have remained constant, and therefore many simulations today are stiff based on the fundamental components of Cycle 400. The variable things will be related to the hydraulic tube component of the reactor, for this is where the rabbit was irradiated in this particular experiment. The input for the modeling of this experiment contained several different "blocks", of which can be defined below:

- Composition block: This block will define all materials (including HFIR materials, as well as target materials)
- Celldata block: information to process multigroup cross sections
- Depletion: defines which compositions to deplete
- Burndata: defines the power and time steps at a given power
- Opus: makes output plots of each specified composition
- Parm: general parameters for the solver
- Geometry Block: geometric model that specifies dimensions of all materials within boundaries
- Bounds: boundary conditions

For this specific thesis, the pellets inside of the rabbit were all input as cylinders within a larger cylinder (the boundary of the aluminum rabbit). Each was defined according to its individual dimensions and position inside of the rabbit, which was done under the Geometry block of the input file. The first step in defining the material within each pellet, however, was to calculate the atomic densities of nickel, along with impurities within each pellet. Table 7 shows the atomic densities of each nickel isotope in each pellet. In knowing the volume of each specimen and with the aid of the assay of the material obtained (86.31% enriched ^{62}Ni), it was possible to calculate atomic densities of every isotope within each pellet specimen. Because there were more than 150 impurities in the material, each was weighed according to its natural abundance and cross-section. With these key pieces of information, one can calculate the fraction of thermal flux that will survive through the isotope. This provides a basic idea of impurities of importance to include in the input code. Because the nickel material used to construct the pellets was only 86.31% enriched, one must account for the other materials within. Therefore, all nickel isotopes must be included in the input of the model. This includes ^{58}Ni, ^{60}Ni, ^{61}Ni, ^{62}Ni, and ^{64}Ni. While we are concerned with the activation of ^{63}Ni through bombardment of neutrons with the ^{62}Ni isotope, one must also take into account neutron transport through the material itself. Impurities of concern were also included in the transport of neutrons, that being ^{137}Gd and ^{32}S. While the atomic densities of each change only slightly with each pellet specimen because of such small mass differences, the impact on final output is significant. Therefore, it was extremely important to calculate the atomic densities of each impurity in each specimen. These explicit numbers were included in the composition block of the input file, which are recorded in g/cm-barns.

Table 7. Atomic densities of Ni isotopes (g/cm-barn)

Target Specimen	^{58}Ni	^{60}Ni	^{61}Ni	^{62}Ni	^{64}Ni
Solid #1	6.14×10^{-3}	3.40×10^{-3}	3.54×10^{-4}	6.37×10^{-2}	2.22×10^{-4}
Solid #2	5.94×10^{-3}	3.29×10^{-3}	3.43×10^{-4}	6.17×10^{-2}	2.15×10^{-4}
2-mm I.D. #1	6.19×10^{-3}	3.43×10^{-3}	3.58×10^{-4}	6.43×10^{-2}	2.24×10^{-4}
2-mm I.D. #2	6.36×10^{-3}	3.52×10^{-3}	3.67×10^{-4}	6.60×10^{-2}	2.30×10^{-4}
4-mm I.D. #1	6.47×10^{-3}	3.58×10^{-3}	3.74×10^{-4}	6.72×10^{-2}	2.33×10^{-4}
4-mm I.D. #2	6.71×10^{-3}	3.72×10^{-3}	3.88×10^{-4}	6.97×10^{-2}	2.42×10^{-4}

The geometry block of the input was constructed in order to tell the code the specific dimensions inside the reactor, in particular the flux trap and hydraulic tube. Even more specifically, the aluminum rabbit including the designated pellets were defined here. By assigning each pellet an arbitrary number, each was designated with specific dimensions so that the code knew precisely the aluminum rabbit position inside the hydraulic tube. The aluminum rabbit was given dimensions spanning from -2.7782 to 2.7782, with a radius of 0.32385 cm. The capsule was defined as a large cylinder, so that placement of the pellets could then be placed within the larger area. Each solid pellet was defined as its own cylinder placed within this larger region, with axial and radial dimensions stated. The ring specimens were treated as two cylinders. Each ring specimen was split into two cylinders, one to define the larger cylinder and then another to represent the inner cylinder that has been removed. This will be further explored in the media block of the code. For this section, it was necessary to first define their placement within the aluminum rabbit. Again, a random number was assigned to represent each specimen. This would be important later to fill each with its designated material.

Once dimensions were defined, the media block would then designate the material defined in the composition block to each assigned cylinder; That is, by pulling the atomic densities instilled in the composition block, it was possible to fill each specified cylinder with the appropriate materials. The solid pellets were self-explanatory, but the ring targets would be a bit more complicated, filling the larger cylinder with the Ni material, and then filling the inner cylinder with air.

The depletion block simply allows the user to instruct the simulation which mixture to deplete. While the default depletion method TRITON uses is to deplete by power, it also provides a method to override this method by using a constant flux approximation instead. This is useful for specific materials, and absolutely appropriate for the specimen activation

observed in this thesis. This is designated with a "parm=orgnflux" input in the beginning on the text input. This block is fundamentally controlling how ORIGEN conducts its depletion, which is done either by time-varying flux (i.e., deplete by power) or constant flux. In the particular simulation used, a constant flux.

The burndata block specified burnup history for the simulation and includes the average specific power in the mictures, the burn length at a particular power, the down time following the burn period, and the number of cross-section libraries produced per cycle. These were inputted based on the amount of time the target was into the reactor, as well as varying the number of cross-section libraries produced per cycle.

The parm block of the input specifies general parameters for the solver. For the purpose of this experiment, three factors were defined; the number of generations to run, the number of neutrons per generation, and the number of generations to be ignored when collecting results. The greater the number of generations, as well as neutrons per generation, the more accurate the results. For the simulations, the following parameters were set in Table 8. The length of the run-time of the simulation was largely dependent on these parameters defined. For example, a simulation running many more generations and neutrons will take a great length longer, but will contain much less error than the contrary. The trade-off is dependent on the experiment being conducted. Due to the small values that this experiment is working with, it was vital to run a large number of generations and number of neutrons per generation for accuracy.

Table 8. Parm block parameters set for simulation

Generations (GEN)	2550
Number of neutrons/generation (NPG)	10,000
Number of generations to skip (NSK)	50

Combining these all and setting the appropriate parameters, the code is able to then generate a flux profile, thereby indicating how much ^{63}Ni is produced for each specific pellet specimen. From this mass and a few conversions, the specific activity can therefore be calculated, thus supporting the given hypothesis.

CHAPTER IV
RESULTS AND DISCUSSION

The hypothesis of this experiment stated there was a geometrical effect on the production of the specific activity of ^{63}Ni after a two-hour irradiation. This geometrical effect would be reinforced through the higher specific activity produced by annular rings rather than solid pellets with the aid of experimental data, as well as through analytical simulation. These results will be observed in the following subsections.

5.1 Experimental Data

5.1.1 Experimental Results

After post-processing techniques, including dissolution and anion exchange column runs, the samples were sent to analytical, where the amount of ^{63}Ni produced was determined from each sample in Bq, disintegrations/second. From these numbers provided, combined with a dilution factor, and several conversions, the specific activity of each specimen was determined. These results can be seen in Table 9.

Table 9. Analytical results of each pellet

Pellet Size	Experimental Specific Activity (mCi/g Ni)	Experimental Specific Activity (mCi/g ^{62}Ni)
Solid #1	9.14±0.91	10.5±0.11
Solid #2	9.53±0.95	11.0±0.11
2 mm ID #1	9.59±0.96	11.0±0.11
2 mm ID #2	9.56±0.96	11.0±0.11
4 mm ID #1	8.82±0.88	10.1±0.10
4 mm ID #2	9.92±0.99	11.4±0.11

Grouping the pellets according to their geometric shape, the average of their specific activities can be observed in Table 10.

Table 10. Specific activities of specimen averaged according to their geometric shape

Pellet Size	Average Specific Activity (mC/g Ni)	Average Specific Activity (mC/g ^{62}Ni)
Solid	9.34±0.93	10.75±1.1
2-mm I.D.	9.58±0.96	11.0±1.1
4-mm I.D.	9.37±0.94	10.75±1.1

5.1.2 Experimental Discussion

There are two areas of this research that need be addressed in reference to supporting or disproving this thesis. The theory behind this experiment was to prove that a specific activity could be achieved by reducing target thickness i.e. reducing neutron activation within the target interior.

The first set of data to examine are the experimental results. While slight, there is a difference in the specific activity of the annular rings as compared to the specific activity produced in the solid pellets. There is a higher specific activity produced in the annular rings than in the solid specimen (both in mCi/g of Ni material, as well as mCi/g of ^{62}Ni). Observing the mCi/g of Ni material first, there is a 0.3 % increase in the average specific activity after a 2-hour irradiation of ^{62}Ni when considering solid pellets to a 4-mm I.D. annular ring. Even more so, there was an average 2.57% increase in specific activity when irradiating 2-mm I.D. annular rings rather than solid pellets. Referring to Table 9, it is also probable that there is error in one of the 4-mm I.D. pellet calculations, perhaps through column exchange or dissolution, where some material was lost. It is thought that 4-mm I.D. #1 is an outlier, considering all of the other pellets follow an increasing specific activity trend. Consider next the specific activity (mCi/g ^{62}Ni material), thus only observing the activity per unit mass of ^{62}Ni, excluding all other Ni isotopes. Considering the averages, the solid pellets produced the same amount of specific activity as the 4-mm I.D. did, however there is an increase of 2.33 % in specific activity produced in the average of the 2-mm I.D. annular rings. While the increase is minimal, it is important to consider the small amounts of pellets this experiment utilized, as well as the short irradiation time. It is however important to take into account the errors given, which were reported as 10% of the values presented by mass spectrometry.

Based on the given data, it would only be advantageous to consider using annular ring specimen rather than solid pellets. There is no additional cost to constructing a ring specimen rather than a solid specimen. In considering one pellet fabrication, producing a 4-mm I.D. ring provides 81.4 % less used material than in fabrication of a solid pellet. Considering the starting material of 1000 mg used in this experiment, roughly nine 4-mm I.D. rings could

have been constructed (each of ~106.9 g) as opposed to five solid pellets (each of ~193.6 g). Based on the results, it is apparent to see that removal of the interior would be beneficial in specific activity production. Eliminating the center would provide the means to construct more target specimen, thereby optimizing production and reducing cost.

5.2 Simulated Data

5.2.1 Preliminary Analytical Simulation Results

In order to properly model the experiment run in this particular thesis, several geometry and media blocks were input so that the code would identify the configuration of the pellets within the aluminum rabbit. In order to first check the validity of the code, it was essential to check the amount of ^{62}Ni that the code confirmed each separate pellet contained. Table 11 shows the known amounts of ^{62}Ni in each pellet as compared to what the code predicted each to contain.

Table 11. A comparison of known weights and simulation results

Pellet ID	Weight of ^{62}Ni (g)	TRITON Prediction (g)	% Error
Solid #1	0.1671	0.1656	0.90
Solid #2	0.1677	0.1662	0.89
2 mm ID #1	0.1531	0.1517	0.92
2 mm ID #2	0.1525	0.1511	0.90
4 mm ID #1	0.0931	0.0923	0.91
4 mm ID #2	0.0923	0.0914	0.92

In comparing these results, it is important to see that the values are extremely similar, which verifies that the code has the geometry and dimensions of the pellets correct. This was purely a calculation of validity to ensure that before irradiation, the code's calculations on how much material is present is equivalent to how much measured in the laboratory.

5.2.2 Simulation Results

After the appropriate inputs were set as discussed in the Method and Materials section of this thesis, a simulation was performed in order to model the target, as well as the phenomena of flux depression. This would be performed in several different ways, each of which will be discussed in further detail.

The first set of data simulated the effects of each pellet irradiated individually; that is, it simulated each pellet one at a time placed in each position inside the aluminum capsule. For this method of simulation, there will be six sets of data presented, one to represent each target

specimen. Figure 33 is a good representation of each simulation run to adequately test the hypothesis.

Figure 33. Depiction of pellet position inside capsule for each simulation

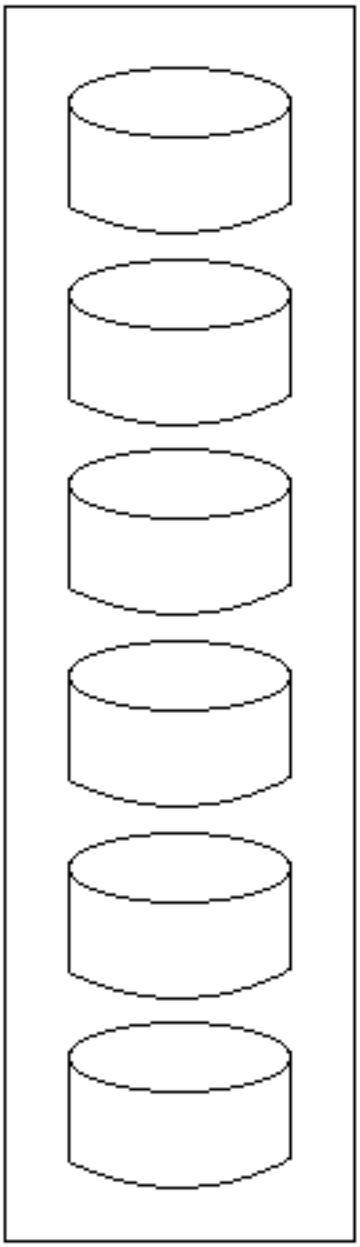

Simulation #1
Solid Pellet #1

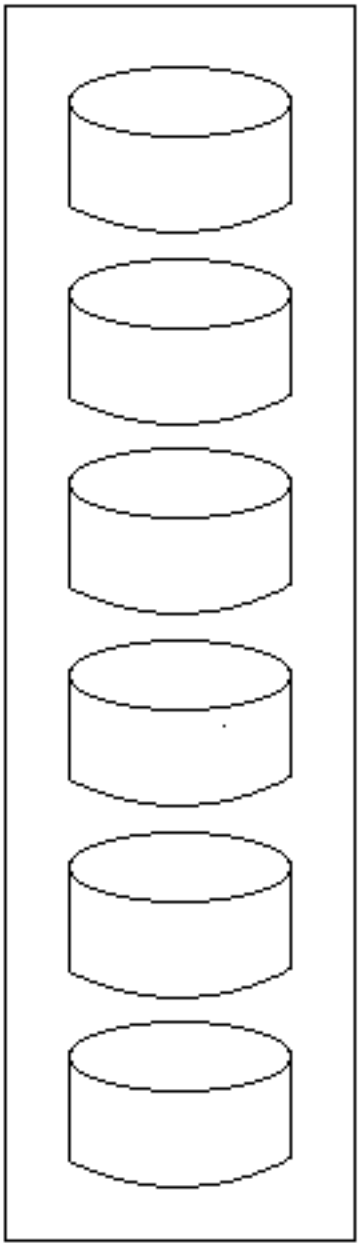

Simulation #2
Solid Pellet #2

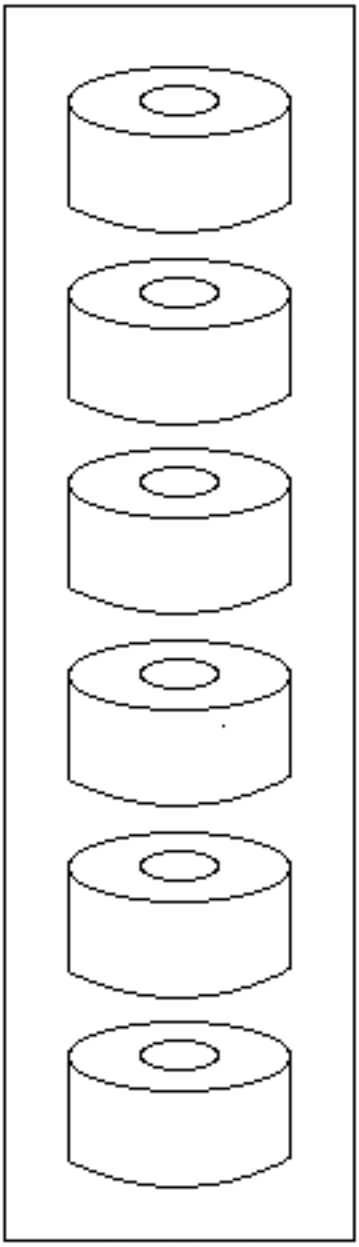

Simulation #3
2-mm I.D. #1

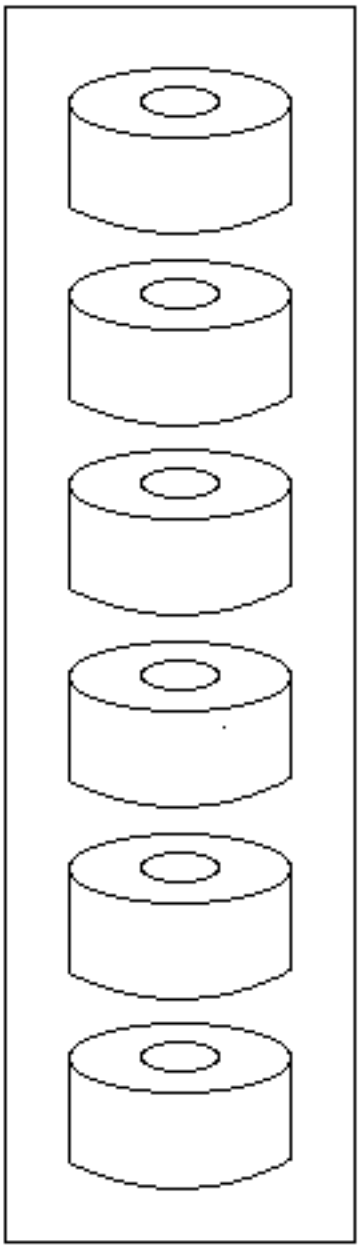

Simulation #4
2-mm I.D. #2

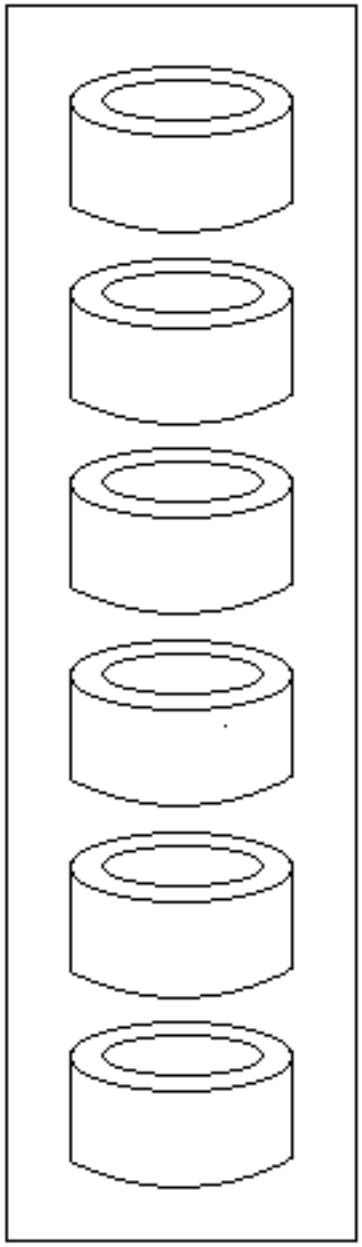

Simulation #5
4-mm I.D. #1

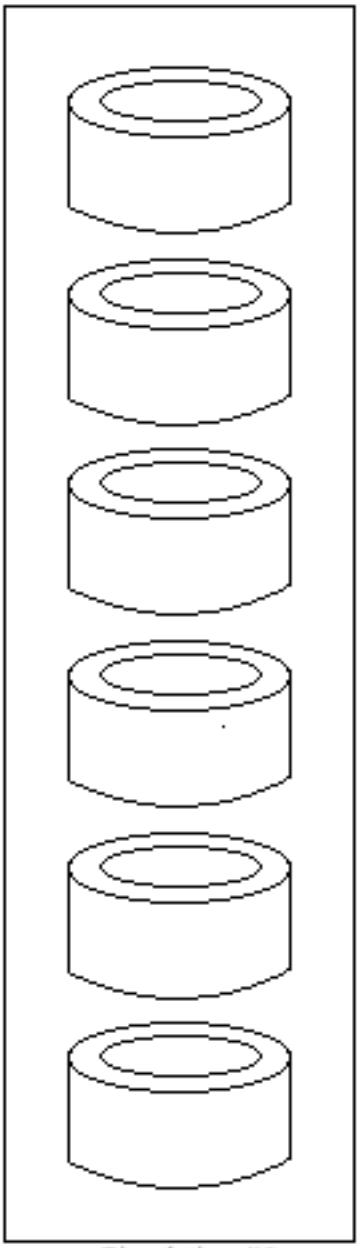

Simulation #6
4-mm I.D. #2

The individual simulations' results as depicted by Figure 33 were tabulated and plotted.

Table 12. Results of analytical simulation #1

Simulation #1 Solid #1 in all positions		
Target Position	Specific Activity (mCi/g Ni)	Specific Activity (mCi/g ^{62}Ni)
Position #1	7.73	8.88
Position #2	7.76	8.92
Position #3	7.88	9.06
Position #4	7.85	9.03
Position #5	7.63	8.77
Position #6	7.99	9.19

Table 13. Results of analytical simulation #2

Simulation #2 Solid #2 in all positions		
Target Position	Specific Activity (mCi/g Ni)	Specific Activity (mCi/g ^{62}Ni)
Position #1	8.09	9.31
Position #2	7.78	8.95
Position #3	7.42	8.54
Position #4	7.25	8.35
Position #5	8.07	9.29
Position #6	8.41	9.68

Table 14. Results of analytical simulation #3

Simulation #3 2-mm I.D. #1 in all positions		
Target Position	Specific Activity (mCi/g Ni)	Specific Activity (mCi/g ^{62}Ni)
Position #1	8.53	9.82
Position #2	8.05	9.26
Position #3	7.98	9.18
Position #4	7.69	8.84
Position #5	7.82	9.00
Position #6	7.76	8.93

Table 15. Results of analytical simulation #4

Simulation #4 2-mm I.D. #2 in all positions		
Target Position	Specific Activity (mCi/g Ni)	Specific Activity (mCi/g ^{62}Ni)
Position #1	8.47	9.75
Position #2	7.99	9.19
Position #3	7.63	8.77
Position #4	8.16	9.39
Position #5	7.94	9.14
Position #6	8.38	9.64

Table 16. Results of analytical simulation #5

Simulation #5 4-mm I.D. #1 in all positions		
Target Position	Specific Activity (mCi/g Ni)	Specific Activity (mCi/g ^{62}Ni)
Position #1	9.02	10.38
Position #2	8.48	9.76
Position #3	8.70	10.01
Position #4	9.02	10.37
Position #5	8.53	9.81
Position #6	8.48	9.76

Table 17. Results of analytical simulation #6

Simulation #6 4-mm I.D. #2 in all positions		
Target Position	Specific Activity (mCi/g Ni)	Specific Activity (mCi/g ^{62}Ni)
Position #1	8.84	10.17
Position #2	8.50	9.78
Position #3	8.57	9.86
Position #4	8.63	9.93
Position #5	8.40	9.67
Position #6	8.34	9.60

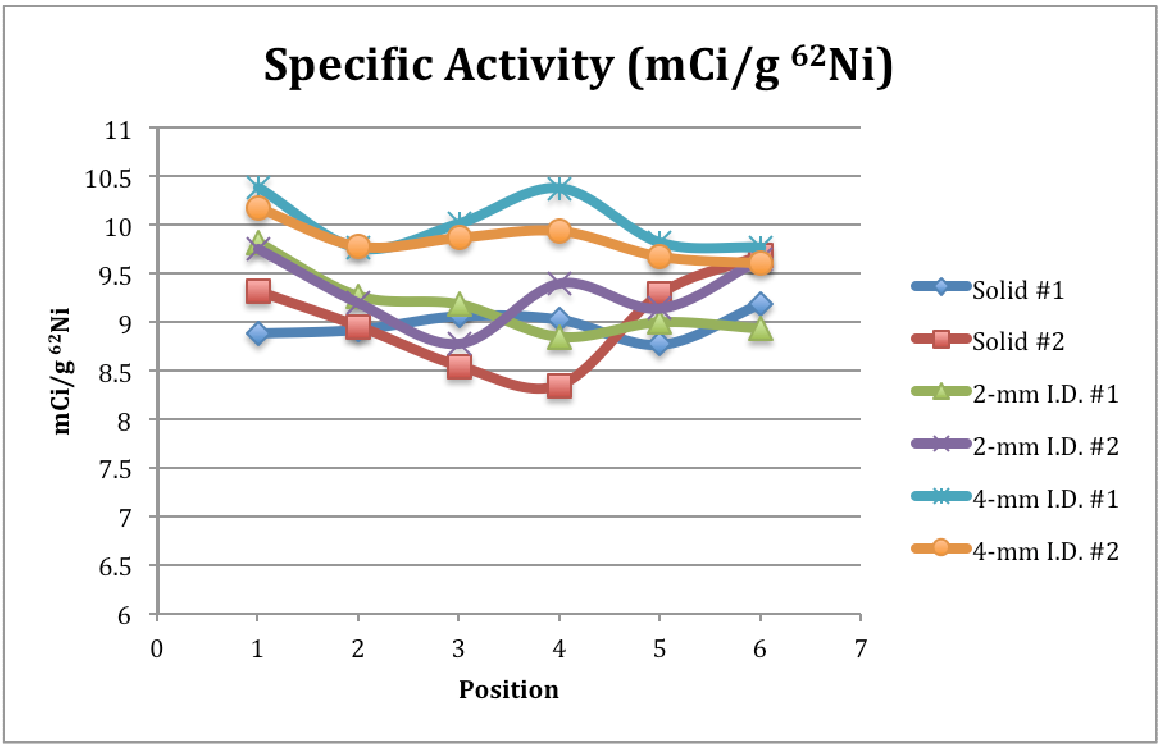

Figure 34. Specific activity (mCi/g ^{62}Ni) as a function of position

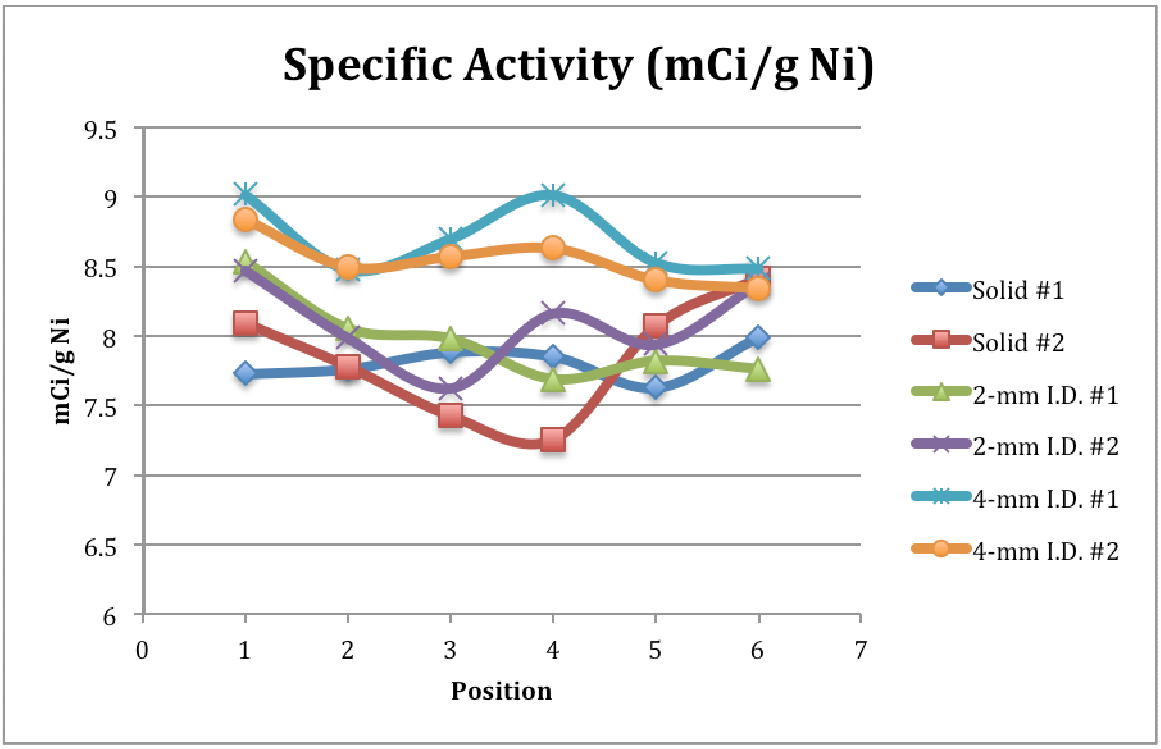

Figure 35. Specific activity (mCi/g Ni) as a function of position

In this set of data, the main thing to consider was the specific activities across each position. Because there was statistical fluctuation observed in the axial positioning of the targets, each separate pellet constructed was observed in every position of the target in order to minimize error. Table 18 shows each position of the target with specific activities of each pellet included in each group.

Table 18. Specific activities of specimen grouped by target position

	Position 1	Position 2	Position 3	Position 4	Position 5	Position 6
Solid #1	7.73	7.76	7.88	7.85	7.62	7.99
Solid #2	8.09	7.78	7.42	7.25	8.07	8.41
2-mm ID #1	8.53	8.05	7.98	7.69	7.82	7.76
2-mm ID #2	8.48	7.99	7.63	8.16	7.94	8.38
4-mm ID #1	9.02	8.48	8.70	9.02	8.53	8.48
4-mm ID #2	8.84	8.50	8.57	8.63	8.40	8.34

For comparison, the averages of each group of specimen (solid, 2-mm I.D., 4-mm I.D.) were taken in order to get a general idea of the geometrical effect on specific activity. These results can be seen in Table 19.

Table 19. Average specific activities of simulations 1-6

Pellet Size Averages	Average specific activity (mCi/g Ni)	Average specific activity (mCi/g ^{62}Ni)
Solid Pellet	7.82±0.31	9.00±0.36
2-mm I.D. rings	8.03±0.30	9.24±0.35
4-mm I.D. rings	8.63±0.23	9.93±0.26

Combining the results from Table 12-17, along with plotting the averages from Table 19, a graphical interpretation can be seen of the data in Figures 36 and 37.

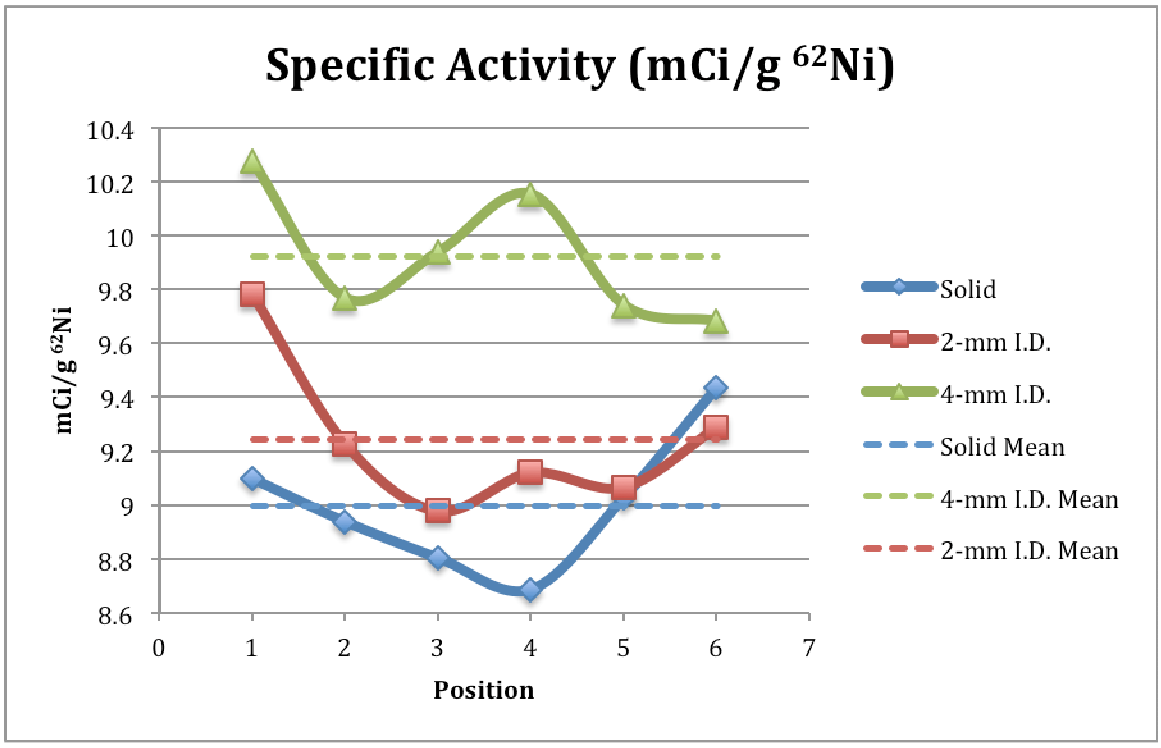

Figure 36. Average specific activities (mCi/g ^{62}Ni) as a function of position

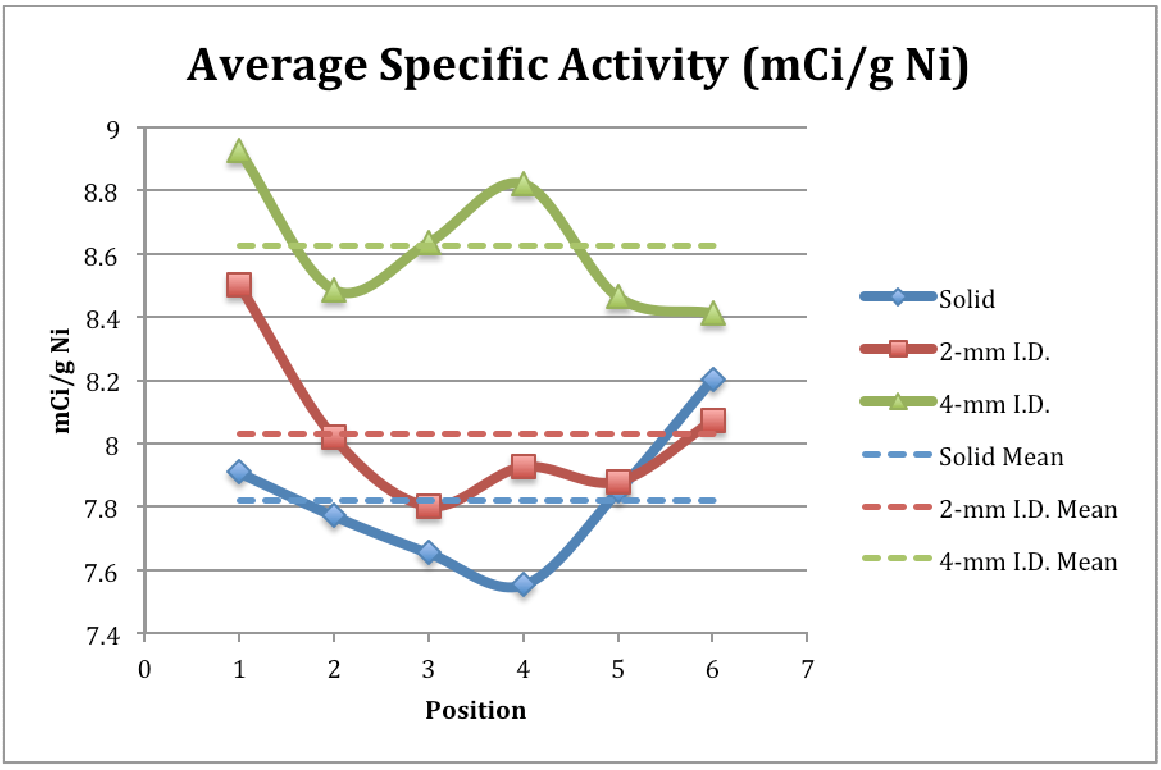

Figure 37. Average specific actvities (mCi/g Ni) as a function of position

Due to statistical fluctuation from the Monte Carlo transport code (refer back to the Simulation Theory section), this was found to be the best method in order to adequately prove the hypothesis of this particular experiment. However, for validity, the actual rabbit, NM-802, was modeled as well. It was input according to Figure 16. The results of the simulation can be seen in Table 20 and Table 21.

Table 20. Target NM-802 specific activities

Pellet Size	Specific activity (mCi/g Ni)	Specific activity (mCi/g ^{62}Ni)
Solid #1	7.89	9.08
Solid #2	7.97	9.17
2-mm ID #1	8.89	10.23
2-mm ID #2	8.83	10.16
4-mm ID #1	8.91	10.25
4-mm ID #2	8.98	10.34

Table 21. Averaged results grouped by size of NM-802 simulation

Pellet Size Averages	Average specific activity (mCi/g Ni)	Average specific activity (mCi/g ^{62}Ni)
Solid Pellet	7.93	9.13
2-mm I.D. rings	8.86	10.20
4-mm I.D. rings	8.95	10.30

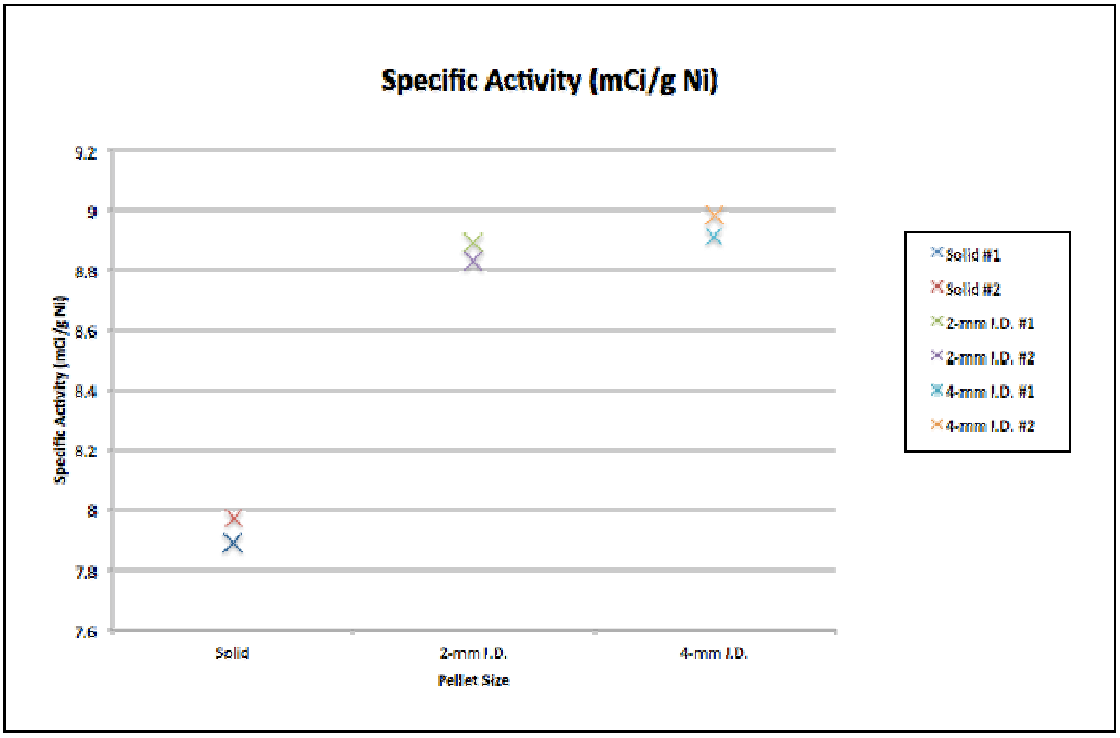

Figure 38. Specific activities of ecah set of specimen (NM-802)cimen

5.2.2 Simulation Discussion

While the data in Figure 38 proved to be important, it was most advantageous to simulate each situation based on pellet size in order to thus prove the hypothesis annular rings would produce more specific activity than the solid pellet specimen. Due to statistical fluctuations in the code, it becomes difficult to simulate a target encasing pellets of different size due to fluctuations in such small specific activities axially. For this reason, each individual pellet (Solid #1, Solid #2, 2-mm I.D. #1, 2-mm I.D. #2, 4-mm I.D. #1, and 4-mm I.D. #2) was placed in each of the six positions that were occupied by the original target irradiated by the pellets fabricated. Figure 32 shows each of the six simulations. This way each position could be compared radially, rather than axially, where most of the fluctuation amongst specific activities was seen. In observing Tables 12-17, while a greater specific activity was experienced in the ring specimen as opposed to the pellets, there are still fluctuations axially, in the different positions. For a summary of specific activities, the average of the different sized specimen can be seen in Table 21. There is an increase in both the activity per unit mass of all nickel isotopes, as well as activity per unit mass of ^{62}Ni (which is expected due to isotopic composition of the material). There is a 3% increase in irradiation of the 2-mm I.D. rings over the solid pellets, and even more a 10% jump in going from solid pellets to the 4-mm I.D. rings. When comparing each position of the capsule, it is evident that there is an increasing trend in specific activity as the center of the pellet is removed, as the area in which air occupies becomes larger.

It should also be noted that there are no errors associated with each value. This is attributed to the fact that propagation of Monte Carlo uncertainties in depletion calculations has not yet been resolved. For this reason the impact of KENO statistical uncertainties on the concentration of ^{63}Ni, as well as errors caused by nuclear data uncertainties, cannot be determined. Mark Williams of Oak Ridge National Laboratory is working on this issue. It was suggested to run several KENO cases using different initial random number seeds, and then computes the standard deviation from the distribution of ^{63}Ni concentrations output in all cases, however for the sake of this thesis, it was not performed.

Consider next the simulation, which modeled the actual target, NM-802. This consisted of one simulation, which placed the pellet specimen as according to Figure 16, alternating the pellet sizes with spacers in between. As expected, the specific activity increases as the pellet interior is diminished. The 2-mm I.D. rings were producing, on average, an increase of 11.7% as compared to the solid pellets. Additionally, when further lessening the pellet interior to a 4-mm I.D. ring, a 12.8% increase was observed as compared to solid pellet production. There was a 0.95% increase in specific activity in the 4-mm I.D. rings than in the 2-mm I.D. rings.

Both methods of model simulation proved that the annular rings, on average, produced a higher specific activity. For this reason, it would only make sense to fabricate and irradiate annular rings in the placement of solid pellets.

CHAPTER V
CONCLUSIONS AND RECOMMENDATIONS

This thesis presented the theory behind the geometrical effect of flux depression in the irradiation of ^{62}Ni pellets and ring specimen in order to produce ^{63}Ni. In addition to proving the hypothesis that annular rings would produce more activity per mass of material experimentally, it also simulated the phenomena using a Monte Carlo depletion code. The simulated results also proved the theory this thesis presented.

Moving forward, additional experimental data is in the works as to further support this hypothesis. Rather than the construction of nickel pellets and rings, a layer of foils, equivalent in dimension, were constructed and placed in an aluminum rabbit. Following the same QA procedures, it underwent the same procedures and tests in order to be subject to irradiation. The aluminum capsule, encasing the nickel foils, was irradiated for the same amount of time as NM-802 and now sits in Building 4501 at Oak Ridge National Laboratory. Dissolution of the foils will indicate and further test that flux depression is present, as to neutron absorption in the outer foils. The inner foils will most likely show little activation. The foils can be modeled in the same way, rather with different geometry and media inputs.

It is the intent of the author that this thesis act as a record and an example to future students who will continue to study the phenomena of flux depression and ^{63}Ni. Additionally, this research can be applied to other elements in isotope production. Information useful to isotope production, flux depression, and simulation theory can be found in the sections discussing the neutron shadowing, and experimental results.

LIST OF REFERENCES

[1] undefined. (August 28, 2012). Radioisotopes Commonly Used in Devices by Industry. In U.S. Environmental Protection Agency. Retrieved July 5, 2012, from http://www.epa.gov/rpdweb00/source-reduction-management/radionuclides.html.

[2] Cooper, S. D.; Moseley, M. A.; Pellizzari, E. D., Analytical Chemistry 1985, 57 (13), 2469-2473.

[3] Tsvetkov, L. A., Pustovalov, A. A., Gusev, V. V., Baranov, V. Y., & Tikhomirov, A. V. (2005). Possible Way To Industrial Production of Nickel-63 and the Prospects of Its Use. *isotope.info | Everything you want to know and learn about isotopes*. Retrieved July 5, 2012, from http://isotope.info/wp-content/uploads/2008/04/possible-way-to-industrial-production-of-nickel-63-and-the-prospects-of-its-use.pdf

[4] Reactor Research Division 2005. Oak Ridge National Laboratory. March 2005 <neutrons.ornl.gov/organization/division_rrd.shtml>

[5] Department of Energy (1993). Self-Shielding. *DOE FUNDAMENTALS HANDBOOK NUCLEAR PHYSICS AND REACTOR THEORY*, *2*(2), 16. Retrieved from http://nuclearpowertraining.tpub.com/h1019v1/css/h1019v1_120.htm.

[6] Turner, J. E. (2007). Neutrons, Fission, and Criticality. In *Atoms, radiation, and radiation protection* (3rd ed., p. 215). Weinheim: Wiley-VCH.

[7] Evaluated Nuclear Data File ENDF/B-V (available from and maintained by the National Nuclear Data Center of Brookhaven National Laboratory).

[8] Thermolyne (n.d.). Type F21100 Tube Furnace. *National Institute of Standards and Technology*. Retrieved August 5, 2012, from http://www.nist.gov/ncnr/upload/E133tubefurnace.pdf

[9] Kth Royal Institute of Technology (2012, October 15). The Bateman equations KTH Reactor Physics, Reaktorfysik, Kungl Tekniska högskolan. *Reactor Physics*. Retrieved from http://neutron.kth.se/courses/transmutation/Bateman/Bateman.html

[10] Rinard, P. (n.d.). Neutron Interactions with Matter. *Federation of American Scientists*. Retrieved August 7, 2012, from http://www.fas.org/sgp/othergov/doe/lanl/lib-www/la-pubs/00326407.pdf

[11] Penn State College of Engineering (n.d.). The Neutron Transport Equation. *Penn State College of Engineering*. Retrieved November 2, 2012, from http://www.engr.psu.edu/cde/courses/nuce521/nuce521_chapter1_reading.pdf

[12] Urbatsch, T. J. (1995). Iterative Acceleration Methods for Monte Carlo and Deterministic Criticality Calculations. Retrieved from http://www.fas.org/sgp/othergov/doe/lanl/lib-www/la-pubs/00326010.pdf.

[13] I. C. Gauld and O. W. Hermann and R. M. Westfall, *ORIGEN-S: SCALE SYSTEM MODULE TO CALCULATE FUEL DEPLETION, ACTINIDE TRANSMUTATION, FISSION PRODUCT BUILDUP AND DECAY, AND ASSOCIATED RADIATION SOURCE TERMS*, ORNL/NSTD/TM-2005/39, Oak Ridge National Laboratory, January 2009.

[14] M. D. DeHart. *TRITON: A TWO-DIMENSIONAL TRANSPORT AND DEPLETION MODULE FOR CHARACTERIZATION OF SPENT NUCLEAR FUEL,* ORNL/NSTD/TM-2005/39, Oak Ridge National Laboratory, January 2009.

[15] D.F. Hollenbach and L.M. Petrie and S. Goluoglu and N.F. Landers and M.E. Dunn, *KENO-VI: A GENERAL QUADRATIC VERSION OF THE KENO PROGRAM,* ORNL/NSTD/TM-2005/39, Oak Ridge National Laboratory, January 2009.

[16] N. Xoubi and R. T. Primm III, *MODELING OF THE HIGH FLUX ISOTOPE REACTOR*

CYCLE 400, ORNL/RRD/TM-2004/251, Oak Ridge National Laboratory, August 2005.

[17] Tutorial 4.2 — Liquid Scintillation Counting. (n.d.). *US Environmental Protection Agency*. Retrieved November 30, 2012, from http://www.epa.gov/safewater/radionuclides/training/transcripts/tutorial_4.2.pdf

[18] Risø National Laboratory for Sustainable Energy (n.d.). Liquid Scintillation Counting for the Determination of Beta Emitter — Principle and Application. *NKS.org Welcome*. Retrieved December 6, 2012, from http://www.nks.org/download/seminar/2009_radworkshop/NKS-B_RadWorkshop_8.pdf

[19] D. F. Hollenbach and J. A. Bucholz, Theoretical Background for Calculational Methods in Scale, ORNL/NSTD/TM-2005/39, *Oak Ridge National Laboratory*, January 2009.

VITA

Spenser Walsh was born to Robert and Sharon Walsh in Seattle, Washington. After graduating from Oak Ridge High School, she went on to receive her bachelor's degree in Radiological Nuclear Engineering at the University of Tennessee, Knoxville. She continues to pursue her doctorate there now.